AD-A185 353 THREE-DIMENSIONAL DYNAMIC LABYRINTH SEAL ANALYSIS(U) 1/1
SCIENTIFIC RESEARCH ASSOCIATES INC GLASTONBURY CT
Y T CHAN ET AL. 02 JAN 87 SRA-910017 AFWAL-TR-87-2009
UNCLASSIFIED F33615-86-C-2665 F/G 11/1 NL

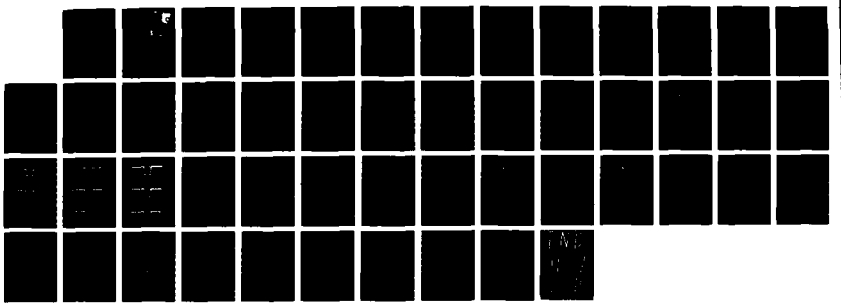

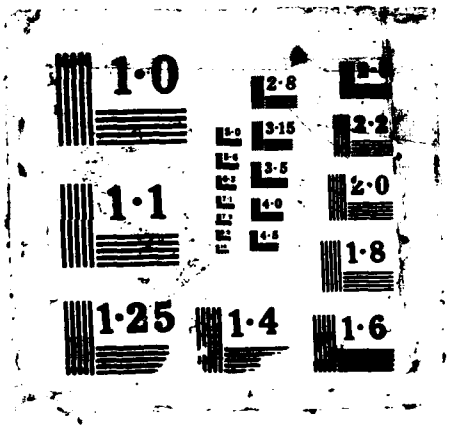
1·0
1·1
1·25
1·4
1·6
1·8
2·0
2·2
2·8
3·15
3·5
4·0

AFWAL-TR-87-2009

THREE-DIMENSIONAL DYNAMIC LABYRINTH SEAL ANALYSIS

Y. T. Chan
R. C. Buggeln
H. McDonald

SCIENTIFIC RESEARCH ASSOCIATES, INC.
P. O. BOX 1058
GLASTONBURY, CONNECTICUT 06033

JANUARY 1987

FINAL REPORT FOR PERIOD JULY 1986 - DECEMBER 1986

AERO PROPULSION LABORATORY
AIR FORCE WRIGHT AERONAUTICAL LABORATORIES
AIR FORCE SYSTEMS COMMAND
WRIGHT PATTERSON AIR FORCE BASE, OHIO 45433

UNCLASSIFIED

SECURITY CLASSIFICATION OF THIS PAGE

A185 353

REPORT DOCUMENTATION PAGE

1a. REPORT SECURITY CLASSIFICATION: Unclassified	1b. RESTRICTIVE MARKINGS: N/A
2a. SECURITY CLASSIFICATION AUTHORITY: N/A	3. DISTRIBUTION/AVAILABILITY OF REPORT: Approved for public release, distribution unlimited
2b. DECLASSIFICATION/DOWNGRADING SCHEDULE: N/A	
4. PERFORMING ORGANIZATION REPORT NUMBER(S): SRA-910017	5. MONITORING ORGANIZATION REPORT NUMBER(S): AFWAL-TR-87-2009
6a. NAME OF PERFORMING ORGANIZATION: Scientific Research Associates, Inc. / 6b. OFFICE SYMBOL (If applicable):	7a. NAME OF MONITORING ORGANIZATION: Aero Propulsion Laboratory (AFWAL/POTX) Air Force Wright Aeronautical Laboratories
6c. ADDRESS (City, State and ZIP Code): P.O. Box 1058 Glastonbury, CT 06033	7b. ADDRESS (City, State and ZIP Code): Wright Patterson AFB, OH 45433
8a. NAME OF FUNDING/SPONSORING ORGANIZATION: Aero Propulsion Laboratory Air Force Wright Aeronautical / 8b. OFFICE SYMBOL (If applicable): AFWAL/ POTX	9. PROCUREMENT INSTRUMENT IDENTIFICATION NUMBER: F33615-86-C-2665
8c. ADDRESS (City, State and ZIP Code): Wright-Patterson AFB, OH 45433	10. SOURCE OF FUNDING NOS.

PROGRAM ELEMENT NO.	PROJECT NO.	TASK NO.	WORK UNIT NO.
62203F	3005	20	61

11. TITLE (Include Security Classification): 3-D Dynamic Labyrinth Seal Analysis

12. PERSONAL AUTHOR(S): Y.T. Chan, R.C. Buggeln and H. McDonald

13a. TYPE OF REPORT	13b. TIME COVERED	14. DATE OF REPORT (Yr., Mo., Day)	15. PAGE COUNT
Final	FROM 7/1/86 TO 12/31/86	87Jan02	37

16. SUPPLEMENTARY NOTATION

17. COSATI CODES			18. SUBJECT TERMS (Continue on reverse if necessary and identify by block number)
FIELD	GROUP	SUB. GR.	Labyrinth Seal, Navier-Stokes Equations, Computational Fluid Mechanics, Alternating Direction Implicit

19. ABSTRACT (Continue on reverse if necessary and identify by block number)

A transient capability has been developed for fluid flow analysis in a labyrinth seal configuration with a whirling rotor. The technique utilizes a moving coordinate system that allows transient calculations of the flow and pressure fields. Two sample calculations with different rotor oscillation displacements are presented and the results demonstrate the potential of this analysis.

20 DISTRIBUTION/AVAILABILITY OF ABSTRACT	21. ABSTRACT SECURITY CLASSIFICATION
UNCLASSIFIED/UNLIMITED ☒ SAME AS RPT ☐ DTIC USERS ☐	Unclassified

22a NAME OF RESPONSIBLE INDIVIDUAL	22b TELEPHONE NUMBER (Include Area Code)	22c OFFICE SYMBOL
1 Lt. Gary F. Willmes	(513) 255-8210	AFWAL/POTX

DD FORM 1473, 83 APR EDITION OF 1 JAN 73 IS OBSOLETE

TABLE OF CONTENTS

1. Introduction

The present trend of aircraft gas turbine design has been characterized by significant increase in cycle pressure ratio and turbine inlet temperatures required to provide higher thermal and propulsive efficiencies. Also, increased interest in engine performance and fuel economy has created additional emphasis for improving the efficiency of gas turbine engines. These trends accentuate the need for improvements in sealing technology and the development of advanced design and analysis capabilities to reduce gas path seal leakage, maintain costly vent leakage to a minimum, provide better control over sophisticated cooling circuits, and prevent high levels of seal leakage into critical aerodynamic locations in the turbine gas path which can result in a considerable penalty from thermal and momentum losses. Advanced gas turbine engine requirements include a broad engine power operating range, which usually results in a wide range of seal clearance. In setting the design clearance, consideration is given to transient differential growth, maneuver deflections, mechanical and thermal growths, eccentricity, and manufacturing tolerances. However, with variable geometry engines and multiple role applications, the engine seals will not always operate at the design clearance nor provide minimum leakage across the operating spectrum. Improved seal design and analysis capabilities developed to address this problem would have a major beneficial impact upon the design. The result of increased cycle pressure ratio on typical labyrinth seal leakage with no change in seal design technology is nearly linear, roughly doubling as the pressure ratio is doubled. These increases are significant, particularly when the number of seals in a gas turbine are considered. Gas turbines require a variety of labyrinth seal designs. The seal configuration selected for a given application is based on the purpose of the seal and satisfying design criteria that includes the following considerations: axial envelope available, axial travel, clearance range, potential wear, system sensitivity to seal clearances, cooling flow requirements, sensitivity to damage in handling, assembly requirements, and pressure ratio.

Labyrinth seals are used throughout a gas turbine engine, including: compressors and turbine airfoil end seals, bearing compartment seals, and flow system seals to prohibit or control flow. The purposes of these seals are not always the same. Labyrinth seals used in the flow path are intended to

minimize end leakage. Bearing compartment seals are intended to keep the oil in the bearing compartment and to minimize the amount of leakage and heat addition to the oil. Thrust balance labyrinth seals are located radially to provide a desired off setting axial load component to reduce bearing loads to the design level. Other flow system network seals have several functions including: controlling leakage flows either to a minimum or to a level to satisfy disc pumping and thus prevent hot gas recirculation in a cavity, controlling cavity pressure to reduce axial bearing loads, or preventing excessive leakage. Seal geometry variables include knife edge thickness and sharpness, clearance, knife pitch, cavity depth and shape, number of knives, step height, knife location on the step, and knife angle. Aerodynamic parameters that must be considered in seal design include rotational speed, pressure ratio, temperature and Reynolds number.

Seal leakage into the flow path has three loss elements: thermodynamic (bypassing combustor); aerodynamic (re-entry to flow path will alter the design velocity diagram for the compressor or turbine airfoils); parasitic (rotational pumping power required to bring leakage up to disc or mainstream velocity). Improper sealing can result in an inadequate supply of air to cooled hardware, which may produce premature failures. Also, poor sealing could result in high oil consumption and choking or possibly fires in the bearing compartments. In addition, poor sealing will cause the engine to rematch at lower than peak component efficiencies.

The benefits of improved sealing are wisely recognized and show the significant improvements of reduced seal leakage on advanced engines, of order 2% SFC reduction for a 4% reduction in leakage.

The results of improving labyrinth seal technology and reducing leakage may also be expressed in terms of cost trade-offs with other gas turbine components. These trade-offs have shown that sealing improvements to achieve the same level of compressor or turbine component efficiency change are more economical. In addition, there is a significant amount of improvement available for sealing efficiency, whereas the state-of-the-art compressor and turbine component efficiencies have relatively less room for improvement.

If a labyrinth seal design is to be successful for the application intended, an accurate seal design and analysis model is necessary. The design and analysis capabilities available today rely heavily on empirical

relationships, which severely limits the application range. Recently, advanced numerical techniques based upon solution of the governing flow equations, the Navier-Stokes equations, have been used for the labyrinth seal analysis [1,2]. These studies have been limited to cases with two coordinate directions, i.e., cases which assume two-dimensional planar symmetry or axial symmetry. For several of the axisymmetric cases the effect of rotation was considered by the imposition of a rotating boundary and the additional solution of the swirl momentum equation. These efforts have clearly shown the ability of the Navier-Stokes approach to simulate the very complex seal flow field for a variety of practical flow configurations. A very important current problem concerns the damping performance of seals in which the gap height at any azimuthal station varies with time. This can be a result of eccentricity, system vibrations, etc., and represents a very challenging problem. The resulting time varying shaft loading can have a major role in damping the vibration, and thereby changing the shaft critical speed. The focus of the present effort would be to simulate these time-dependent flow fields due to a non-constant gap height via a solution of the time-dependent Navier-Stokes equations.

2. Phase I - Technical Objective

The overall objective of the present effort was to develop a Navier-Stokes analysis which would be applied to two-dimensional, time-dependent labyrinth configurations. While it is realized that the eccentricity or forced vibration problems are inherently three-dimensional in nature, it was felt that the potential of the Navier-Stokes approach could be assessed through consideration of a two-dimensional seal geometry in which the gap heights vary in a prescribed manner with time. An existing code with time invariant geometry was extended to apply to this problem and calculations were run to assess the procedure. The flow fields were interrogated to determine if the approach gives the qualitatively expected effect of gap time-dependence. This approach was taken because of the limited time and resources available under the Phase I effort. Under the Phase II effort, the full three-dimensional time dependent approach would be used to simulate the eccentricity and forced vibration problems. Details of this effort follow.

3. Mathematical Analysis

The flow field within a labyrinth seal is governed by the Navier-Stokes equations, and in conjunction with a suitable turbulence model a solution of the time-dependent form of these equations would serve to predict the flow field for both laminar and turbulent flows. As the present code is configured, the mixing length mdoel assumes that the flow is fully turbulent, i.e., there is no transition from laminar to turbulent flow. The two-equation model, however, does have an inherent transition model within the governing equations and hence, automatically considers the physics of transition. The form of the Navier-Stokes equations expressed in the more common coordinate systems can be found in standard fluid dynamic texts [3], and the equations themselves have been derived in general tensor form by Walkden [4] for viscous flow.

The form considered in this investigation is based upon density, ρ, and the radial and axial velocities, u and w, as dependent variables and continuity and the momentum equations written in the cylindrical polar coordinates as governing equations. In this approach the continuity and momentum equations are solved in the form

$$\frac{\partial(J\vec{W})}{\partial\tau} = -\sum_{j=1}^{3} \frac{\partial}{\partial y^j}\,(Jy^j{}_{,t}\vec{W}) - \sum_{j=1}^{3} \left(\beta_i \frac{\partial}{\partial y^j}\,(Jy^j{}_{,i}\vec{F}_i)\right.$$

$$\left. + \gamma_i \frac{\partial}{\partial y^j}(Jy^j{}_{,i}\,\vec{P}_i) + \zeta_i \frac{\partial}{\partial y^j}\,(Jy^j{}_{,i}\,\vec{G}_i)\right) \qquad (1)$$

$$+ J\vec{C}$$

where

$$y,^j{}_t \equiv \frac{\partial y^j}{\partial t}$$

$$y,^j{}_i \equiv \frac{\partial y^j}{\partial \bar{x}_i} \qquad (2)$$

and J is the Jacobian of the inverse transformation

$$J = \frac{\partial(\bar{x}_1, \bar{x}_2, \bar{x}_3)}{\partial(y^1, y^2, y^3)} = \begin{vmatrix} \frac{\partial \bar{x}_1}{\partial y^1} & \frac{\partial \bar{x}_1}{\partial y^2} & \frac{\partial \bar{x}_1}{\partial y^3} \\ \frac{\partial \bar{x}_2}{\partial y^1} & \frac{\partial \bar{x}_2}{\partial y^2} & \frac{\partial \bar{x}_2}{\partial y^3} \\ \frac{\partial \bar{x}_3}{\partial y^1} & \frac{\partial \bar{x}_3}{\partial y^2} & \frac{\partial \bar{x}_3}{\partial y^3} \end{vmatrix} \tag{3}$$

Further, the coefficients β_i, γ_i, ζ_i are given by

$$\begin{aligned} \beta &= \frac{1}{r}, \quad \beta_2 = \frac{1}{r}, \quad \beta_3 = 1 \\ \gamma_1 &= 1, \quad \gamma_2 = \frac{1}{r}, \quad \gamma_3 = 1 \\ \zeta &= \frac{1}{r^m}, \quad \zeta_2 = \frac{1}{r}, \quad \zeta_3 = 1 \end{aligned} \tag{4}$$

and $m = 1$ for all equations except the x_2 - direction momentum equation, for which $m = 2$. The vector variables used in Eq. 1 are defined as

$$\vec{W} = \begin{bmatrix} \rho U_1 \\ \rho U_2 \\ \rho U_3 \\ \rho \end{bmatrix} \qquad \vec{F}_i = r^n \begin{bmatrix} \rho U_1 U_i \\ \rho U_2 U_i \\ \rho U_3 U_i \\ \rho U_i \end{bmatrix} \tag{5}$$

where $n = 1$ for $i = 1$ and $n = 0$ for $i = 2, 3$.

$$\vec{P}_i = \begin{bmatrix} p\delta_{i1} \\ p\delta_{i2} \\ p\delta_{i3} \\ 0 \end{bmatrix} \qquad \vec{G}_1 = \begin{bmatrix} r\tau_{11} \\ r^2\tau_{12} \\ r\tau_{13} \\ 0 \end{bmatrix} \qquad G_i = \begin{bmatrix} \tau_{i1} \\ \tau_{i2} \\ \tau_{i3} \\ 0 \end{bmatrix} \quad \text{for } i = 2, 3 \tag{6}$$

Note that the velocity components (U_1, U_2, U_3) are the cylindrical-polar velocity components, and τ_{ij} is the stress tensor written in cylindrical-polar coordinates. The molecular and turbulent stress tensors may be written as

$$\tau_{ij} = 2\mu_{eff}\,\bar{D}_{ij} \tag{7}$$

$$\bar{D}_{11} = \frac{\partial U_1}{\partial \bar{x}_1}$$

$$\bar{D}_{22} = \frac{1}{r}\frac{\partial U_2}{\partial \bar{x}_2} + \frac{U_1}{r}$$

$$\bar{D}_{33} = \frac{\partial U_3}{\partial \bar{x}_3} \tag{8}$$

$$\bar{D}_{12} = \frac{1}{2}\left[r\,\frac{\partial}{\partial \bar{x}_1}\left(\frac{U_2}{r}\right) + \frac{1}{r}\frac{\partial U_1}{\partial \bar{x}_2} \right]$$

$$\bar{D}_{13} = \frac{1}{2}\left[\frac{\partial U_3}{\partial \bar{x}_1} + \frac{\partial U_1}{\partial \bar{x}_3} \right]$$

$$\bar{D}_{23} = \frac{1}{2}\left[\frac{1}{r}\frac{\partial U_3}{\partial \bar{x}_2} + \frac{\partial U_2}{\partial \bar{x}_3} \right]$$

$$\nabla \cdot \bar{U} = \frac{1}{r} \frac{\partial}{\partial \bar{x}_1} (rU_1) + \frac{1}{r} \frac{\partial U_2}{\partial \bar{x}_2} + \frac{\partial U_3}{\partial \bar{x}_3} \tag{9}$$

The derivatives required in Eqs. (8) - (9) must be expressed in terms of the computational coordinates y^j using the chain rule.

Finally, the vector $\hat{C}$ contains the additional curvature terms due to the cylindrical-polar coordinate system.

$$\hat{C} = \begin{bmatrix} \frac{1}{r} \rho U_2^2 - \frac{1}{r} \bar{\tau}_{22} \\ - \frac{1}{r} \rho U_1 U_2 \\ 0 \end{bmatrix} \tag{10}$$

Since the present effort involves the problem of turbulent flow, a turbulence model suitable for this problem is necessary. Using Favre averaging [5], the governing equations are then identical to the laminar equations with velocity and density being taken as mean velocity and viscosity as the sum of the molecular and turbulent viscosity. Several models of varying sophistication are available for the turbulent viscosity. The code being used for the present effort contains both a mixing length turbulence model and a two-equation turbulence model. This latter approach is based upon solution of the turbulence energy and dissipation equations in conjunction with the mean flow equations. In the present effort, transition from laminar to turbulent flow occurs far upstream of the first blade and, in fact, the domain where the computation is performed is fully within the turbulent region. Although eventually a two-equation model may be required for this problem, previous experience (Refs. 1 and 2) has shown that many of the essential features of the seal flow field can be captured with a numerical simulation using a mixing length approach. Therefore, since in this effort transition was not of importance and due to the fact that the use of a two-equation model would increase run time by approximately 50%, a mixing length model was used. The mixing length, ℓ_m, was computed from [6].

$$\ell_m = 0.09\Delta \tanh\left(\frac{Ky}{0.09\Delta}\right)D$$

where K is the van Karman constant, y is the distance normal to the wall, Δ is the boundary layer thickness and D is a sublayer damping factor which is determined from the analysis of Van Driest [7]. The turbulent viscosity, μ_T, then was obtained by

$$\mu_T = \rho \ell_m \sqrt{D:D}$$

where D:D is the second invariant of the mean flow rate of deformation tensor. With the mixing length model used, the mixing length will be zero on the wall and will monotonically increase (not linear) through the boundary layer becoming a maximum of 0.09Δ at the edge of the boundary layer and remaining constant thereafter. D:D is a maximum on the wall and will become zero at the edge of a boundary layer. Thus, the combined effort is to produce a turbulent viscosity of zero on the wall, increasing to a maximum with the boundary layer and becoming zero at the edge of the boundary layer.

4. Numerical Analysis

The numerical procedure used to solved the governing equations is a consistently split linearized block implicit scheme originally developed by Briley and McDonald [8] and embodied in a computer code termed MINT, an acronym for Multidimensional Implicit Nonlinear Time-Dependent. The basic algorithm has been further developed and applied to both laminar and turbulent flows. Since the scheme has been described in detail in several publications available in the open literature, it will not be detailed here. Rather, only a brief outline of the procedure will be given in the following.

The governing equations are replaced by an implicit time difference approximation, optionally a backward difference or Crank-Nicolson scheme. Terms involving nonlinearities at the implicit time level are linearized by Taylor series expansion about the solution at the known time level, and spatial difference approximations are introduced. The result is a system of multidimensional, coupled (but linear) difference equations for the dependent variables at the unknown or implicit time level. To solve these difference

equations, the Douglas-Gunn procedure for generating alternating-direction implicit (ADI) splitting schemes as perturbations of fundamental implicit difference schemes is introduced in its natural extension to systems of partial differential equations. This ADI splitting technique leads to systems of coupled linear difference equations having narrow block-banded matrix structures which can be solved efficiently by standard block-elimination methods.

The method centers around the use of a formal linearization technique adapted for the integration of initial-value problems. The linearization technique, which requires an implicit solution procedure, permits the solution of coupled nonlinear equations in one space dimension (to the requisite degree of accuracy) by a one-step noniterative scheme. Since no iteration is required to compute the solution for a single time step, and since only moderate effort is required for solution of the implicit difference equations, the method is computationally efficient; this efficiency is retained for multidimensional problems by using ADI matrix splitting techniques. The method is also economical in terms of computer storage, in its present form requiring only two time levels of storage for each dependent variable. Furthermore, the splitting technique reduces multidimensional problems to sequences of calculations which are one-dimensional in the sense that easily-solved narrow block-banded matrices associated with one-dimensional rows of grid points are produced. Consequently, only these one-dimensional problems required rapid access storage at any given stage of the solution procedure, and the remaining flow variables can be saved on auxiliary storage devices if desired. Since each one-dimensional split of the matrix produces a consistent approximation to the original system of partial differential equations, the scheme is termed a consistently split linearized block implicit scheme. Consistent splitting has been shown by a number of authors [9] to considerably simplify the application of the intermediate split boundary conditions.

The present Phase I effort applied the LBI scheme to a time-dependent body fitted coordinate system simulating flow through a seal with a time varying gap height. At every time step, a boundary fitted coordinate system was constructed to accommodate the time dependent characteristic of the boundary (rotor). A simple Eulerian height function was used to represent the rotor surface. Various techniques to describe a moving surface can be found in Chan and Banerjee [10]. This function is defined as the distance from a reference line and is prescribed by a sinusoidal function in time.

For numerical calculations, the height function is discretized into points, sometimes called markers. These markers are then used to define the time dependent boundaries. Since a boundary fitted coordinate system is used, the boundary is part of the grid system at all times. For this reason, flow variables at the moving boundary are well defined and application of the boundary conditions at these boundaries is straightforward.

The numerical procedure can be summarized in four steps: 1) the governing equations of the fluid and their corresponding boundary conditions are transformed into a boundary fitted coordinate system according to the shapes of the surface; 2) the governing equations are solved in the transformed coordinates using the LBI scheme; 3) locations of the surface are advanced using the prescribed motion of the rotor; and 4) advance time step and repeat the sequence.

5. Results

The work performed in the present Phase I program can be identified by three tasks :

I. Confirmation of the numerical capabilities of the existing MINT code to handle time-dependent sample 10-20X scale labyrinth seal geometries.
II. Numerical calculations using realistic flow conditions.
III. Assessment of the Navier-Stokes approach to the three-dimensional, time dependent labyrinth seal problem.

These three tasks are now discussed in detail.

Task I:

As the first task in the Phase I effort, the existing vectorized coding was verified for cylindrical-polar and time-dependent coordinates. These are the main features of the vectorized code which have not yet been verified but are required for the seal calculations performed here. The code has been written as a general geometry code in which the computational coordinates are a function of the Cartesian or polar coordinates and time. Verification consisted of two parts. In the first part, the cylindrical polar coordinates option was validated through a test case which has an analytical solution for

the fully developed laminar pipe flow. The fluid flow inside a pipe was used to test the cylindrical polar coordinates option of the code. For this case, the Hagen-Poiseuille parabolic velocity distribution was obtained. The calculations agreed to within less than 0.1% with the analytical solution of the Navier-Stokes equations. To assess that the time dependent coordinate option was working properly, a series of detailed printouts including intermediate results, was made. These intermediate printouts showed the code to be correctly evaluating the convective-like terms which are produced by the time movement of the coordinate system.

Task II:

In the second task, three demonstration calculations were made. In these cases a geometry of straight tapered seal with three knives was used. The first calculation obtained a converged solution with time-independent seal boundary. The purpose of this case was to exercise task I on the seal geometry and also serve as initial conditions for cases 2 and 3. Cases 2 and 3 involved calculations of flow field inside the straight tapered seal geometry with a prescribed time dependent boundary (Figure 1). The rotor was chosen to be the time-dependent surface and the motion of it is sinusoidal with time. In these two cases, the moving surface had an oscillatory frequency of one. The amplitude of oscillation of the moving surface in cases 2 and 3 was 0.1 and 0.2, respectively. These amplitudes correspond to a changes of 20% and 40% of the entire gap height.

Since the overall objective of the Phase I effort was to demonstrate the ability of the Navier-Stokes solver to calculate the flow within the seals of an eccentric whirling rotor, a representative seal geometry with which the authors were well acquainted was chosen. For all three cases, fluid flow calculations have been performed in a straight tapered seal configuration with three knives (Figure 1). The clearance of each seal is chosen as a characteristic length, δ, of 0.1 inches (0.245 cm). All other dimensions on Figure 1 are referred as multiples of this length. The stator had a radius of 5.2 inches (13.2 cm). For the cases run under this effort, the governing equations consisted of the transformed streamwise and transverse polar momentum equations and the continuity equation. The initial conditions and boundary conditions can be summarized as the following. The flow is initially assumed to be stagnant and the back pressure lowered to the desired level. The

boundary conditions use the no-slip conditions on the walls, the two-layer model at the inlet, and specified static pressure on the exit boundary. The two layer model divides the upstream inlet boundary into two regions (1) a central core in which the total pressure is specified and (2) a boundary layer region in which the pressure is assumed constant and the form, but not the magnitude, of the boundary layer velocity profile is assumed. The assumed profile is normally determined by specifying a distance from a leading edge and a boundary layer growth rate. Thus a boundary layer thickness is determined at the computational inlet plane and a boundary layer velocity profile is either user specified or determined by a variety of analytical or semi-analytical techniques (e.g., [11-12]). In this study, the method of Maise and McDonald [11] was used. In essence, the boundary layer thickness and the form of the velocity profile represent the upstream history of the flow before entering the region of computation. The edge velocity was determined from the specified inlet total pressure and the static pressure determined via the time-evolving solution. For the cases considered, the pressure ratio was 2.0. The inlet boundary layer profiles on the rotor and land entrance were assumed to have a thickness of 0.05 inches (0.0122 cm) and a skin friction coefficient of 0.005. The turbulence viscosity was assumed to be modeled by a mixing length model previously discussed. Once a steady state was achieved, the rotor is allowed to move in the radial direction.

Figure 2 and 4 show the velocity vector plots and pressure contours inside the blade gaps for case 1. Figure 3 shows the axial velocity profile along the first coordinate line in the first blade gap. In this case, the flow remained subsonic except in a small axial region (65δ to 67δ) near the third knife blade, where δ refers to the gap shown in Fig. 1. The maximum Mach number was 1.03 at an axial location, 65δ, in the third blade gap. This was approximately where the dimensionless pressure is 0.48. A large recirculation exists downstream of the last blade and recirculating zones exist in the two cavity regions, as was expected. A small recirculating vortex was found at the first blade surface. Along all blade surfaces, low pressure points were found at the leading edge of each blade. In the third blade surface, a low pressure point was also observed at the trailing edge. At the exit area of the first, second and third blade, the pressures are 0.64, 0.60 and 0.48 of the inlet pressure, respectively.

In cases 2 and 3, the radial motion of the rotor was assumed to have an oscillatory frequency (in time) of unity. To study the effects due to this moving boundary, pressure and axial velocity near the middle of the third knife blade surface were traced in time both on the blade and the rotor at the position shown in Fig. 1. The results are plotted in Figures 5 and 19 for these cases. Figure 5 shows the pressure and axial velocity for case 2. In this case, the amplitude of oscillation for the rotor was 0.1. This corresponds to a gap height change of 0.9δ to 1.1δ. Approximate periodic solutions were obtained after five transient cycles. In this case and the next set of calculations, the radial velocity of the fluid on the rotor was imposed by the prescribed motion of the rotor. The amplitude of the oscillatory rotor was 0.1. For this location, the pressure variation at the rotor surface was 0.40 of that at the third blade surface and these two pressures had a phase shift of about 45°. Figures 6 - 9 show the coordinates in the three blade gaps at quarter cycles of the motion of the rotor. Notice that the moving coordinates occur in the gap regions only; this is to reduce any unnecessary numerical disturbance in other regions. Figures 10 - 13 show the velocity vectors in the blade gaps at different quarter cycles of the movement of the rotor. Figure 14 shows the axial velocity profiles along the first coordinate line in the first blade gap at different quarter cycles of the movement of the rotor. Small recirculating vortices were found at the first stator blade surface in all situations. The entire flow remained subsonic except in a small region near the exit of the third stator blade. The Mach number in this region varied from 1.06 to 1.1, with the largest value occurring when the rotor was at its first quarter cycle (i.e., when the gap height is one and is on the way to a smaller height). This maximum Mach number occurred at an axial distance of 66δ. Figures 15 - 18 show the pressure contours in the blade gaps at different quarter cycles of the movement of the rotor. The time dependent nature of the flow field is clearly evident in these figures. In particular, Figures 15 and 17 show the same instantaneous gap height with the gap increasing in Figure 17 and decreasing in Figure 15. The pressure contours for these times show significant variation.

In the last case (case 3), the amplitude of oscillatory rotor was chosen to be 0.2. This corresponds to a change of gap height from 0.8δ to 1.2δ. The pressure and axial velocity variation at the starred location is shown in Figure 19. Figures 20 - 23 show the velocity vectors in the blade gaps at

different quarter cycles of the movement of the rotor. Figure 24 shows the axial velocity profiles along the first coordinate line in the first blade gap at different quarter cycles of the movement of the rotor. Small recirculating vortexes were found at the first stator blade surface in the third and fourth quarter cycles only. The Mach number varies from 1.10 to 1.13, with the largest value at the third quarter cycle (when the gap height is one and is on the way to larger gap height). This maximum Mach number occurred at an axial distance of 67δ. Figures 25 - 28 show the pressure contours in the blade gaps at different quarter cycles of the movement of the rotor.

In summary, of the calculations discussed, the first was for a steady state solution. This was also used as an initial condition for the subsequent time-dependent runs. The numerical technique utilized in this first case was to obtain a steady state solution in the most computationally efficient manner without regard for transient accuracy. This was accomplished by a matrix preconditioning technique [13] which can be viewed as taking a fictitious variable time step through the spatial field. For cases 2 and 3, which involved time-dependent solutions, the physical time steps were used to maintain transient accuracy. A constant time step of 0.005 was chosen for these cases. The periodic solution obtained indicates this time step choice to be a viable one.

The converged solution for the first case was obtained in 300 iterations. The pressure was lowered to the ambient value equal to 50 percent of the stagnation value over 25 time steps, and then the case was run to the steady state solution. For cases 2 and 3, with a oscillating land of unit frequency, 200 time steps were required to complete one oscillatory cycle. The CPU time for each time step was 2.25 seconds with 75×150 grid points. A fully vectorized version of MINT code was used for the present calculations.

Task III:

The objective of the present Phase I effort was to perform a preliminary assessment of the capability of a Navier-Stokes code to simulate flow physics of a seal with varying gap and to assess the practicality of such a procedure. Considering the latter item first, a periodic solution was obtained in 1125 seconds of CRAY-XMP CPU time. This run time is within range to allow simulations of large numbers of selected cases. Further, since no study of maximum allowable time step has been made, it is possible that the allowable time step could be increased considerably, thus shortening required run time.

In regard to the results, periodic solutions were clearly obtained. This is most dramatically shown by comparison of pressure distributions for the same gap height at times 180° apart in the cycle (Figures 15 and 17). In regard to an approximate assessment of the results, it is possible to consider the present two-dimensional calculation as simulating some features of the actual three-dimensional case. This can be done by considering the instantaneous solution at any time to correspond to the solution for the three-dimensional problem at the azimuthal location having the same gap height. The net force acting on the rotor can then be calculated from the pressure at the rotor in one cycle of oscillation.

The net forces acting on the rotor are calculated for each case (2 and 3). In case 2, the calculated net force (average dynamic centering force) is 3.2 N and is acting at an angle of 141.5° (see Figure 29). By assuming an average radius of whirl orbit of 0.16 inches, the radial stiffness, $K_{sb}=F/r$, is 12.6 KN/m. The radial stiffness in a similar situation [14] is obtained experimentally in the range of 0 to 25 KN/m over a range of frequencies and pressure gradients. Our two-dimensional approximation to a whirling rotor case thus provides a qualitatively satisfactory result.

6. Conclusions

Under the present effort, a transient capability has been developed which enables a designer to calculate the flow in a labyrinth seal configuration with an eccentric whirling rotor. This has been done by solving the transient Navier-Stokes equations in a coordinate system which reflects the seal gap variation as a function of time. This new capability has been incorporated within a very general two- and three-dimensional Navier-Stokes procedure which has been applied previously to a wide variety of turbomachinery flow problems. Typical examples have been seals with and without swirl, disk pumping cavities, cascades, etc. Although the analyses have been confined to equations written in an inertial frame, extension to a rotating frame is straighforward. Therefore, the basic code can now effectively simulate a large number of relevent flow fields.

In regard to the work considered specifically under this effort, calculations were made in an axisymmetric simulation for a sinusoidally varying gap height at two frequencies. Periodic flow was obtained in both cases with

five cycles of motion. The computed flow fields were examined and the results appeared physically realistic. Obviously, a detailed comparison with experiment for three-dimensional configurations of interest is required before a quantitative assessment can be made. The basic procedure has been applied to a variety of three-dimensional problems and application to a seal problem which has time-dependent gap height and is not axisymmetric, i.e., fully three-dimensional, should be relatively straightforward.

The present SRA Navier-Stokes code represents a state-of-the-art procedure in simulating highly resolved complex flow fields. The procedure is based upon an efficient ADI approach which allows high near wall resolution and significant grid stretching; both of these properties are required to compute the complex flow present in turbomachinery. The code itself is highly vectorized, leading to very short run times per grid point per time step. For steady state solutions, the code contains matrix reconditioning techniques which lead to very rapid convergence. Typically, convergence is obtained within 100 to 300 time steps for flows having near wall resolution and a large number of grid points. These properties make the code very suitable for application to complex turbomachinery flow problems.

7. References

1. Buggeln, R.C. and McDonald, H.: Development of a Navier-Stokes Analysis for Labyrinth Seals, AFWAL-TR-85-2103, 1985.

2. Buggeln, R.C., Roscoe, D.V., Kim, Y.N., McDonald, H.: Solution of The Navier-Stokes Equations For The Flow in Advanced Labyrinth Seals, AFWAL-TR-85-2038, 1985.

3. Schlichting, H.: Boundary Layer Theory, McGraw Hill Co., New York, 1960.

4. Walkden, F.: The Equations of Motion of a Viscous, Compressible Gas Referred to an Arbitarily Moving Coordinates System, Royal Aircraft Est. Tech. Paper #66140, 1966.

5. Favre, A.J.: The Equations of Compressible Turbulent Gases, Annual Summary Report #1, Institute de Mechanique Statistique de la Turbulence, 1965.

6. McDonald, H. and Camarata, F.J.: Computation of Turbulent Boundary Layers - 1968 AFOSR-IFP Stanford Conference, Vol. I, Ed. S.J. Kline, M.V. Markovin. G. Sovran and D.J. Cockrell, Stanford University, 1969, pp. 82-98.

7. van Driest, E.R.: On Turbulent Flow Near Wall, J. Aero Sci., Nov. 1956

8. Briley, W.R., McDonald, H: Solution of the Multidimensional Compressible Navier-Stokes Equations by a Generalized Implicit Method, J. Comp. Phys. Vol. 24, 1977, pp. 372-397.

9. Briley, W.R., McDonald, H: On the Structure and Use of Linearized Block Implicit Schemes, J. Comp. Phys., Vol. 34, 1980, pp. 54-72.

10. Chan, Y.T., Banerjee, S: Vortex Methods for Free Interface Problems, Nucl. Sci. & Eng., Vol. 93, 1986, pp. 62.

11. Maise, G. and McDonald H.: Mixing Length and Kinematic Eddy Viscosity in a Compressible Boundary Layer. AIAA Journal, Vol. 6, No. 1, January 1968, pp. 73-80.

12. Musker, A.J.: Explicit Expression for Smooth Wall Velocity Distribution in a Turbulent Boundary Layer, AIAA Journal, Vol. 17, 1976.

13. Briley, W.R., Buggeln, R.C. and McDonald, H.: Solution of the Three-Dimensional Navier-Stokes Equations for a Steady Laminar Horsehoe Vortex Flow, SRA Report R84-920014-f, ONR, December 1984.

14. Wright, D.V.: Labyrinth Seal Forces on a Whirling Rotor, NASA Contractor Report 168016, 1983.

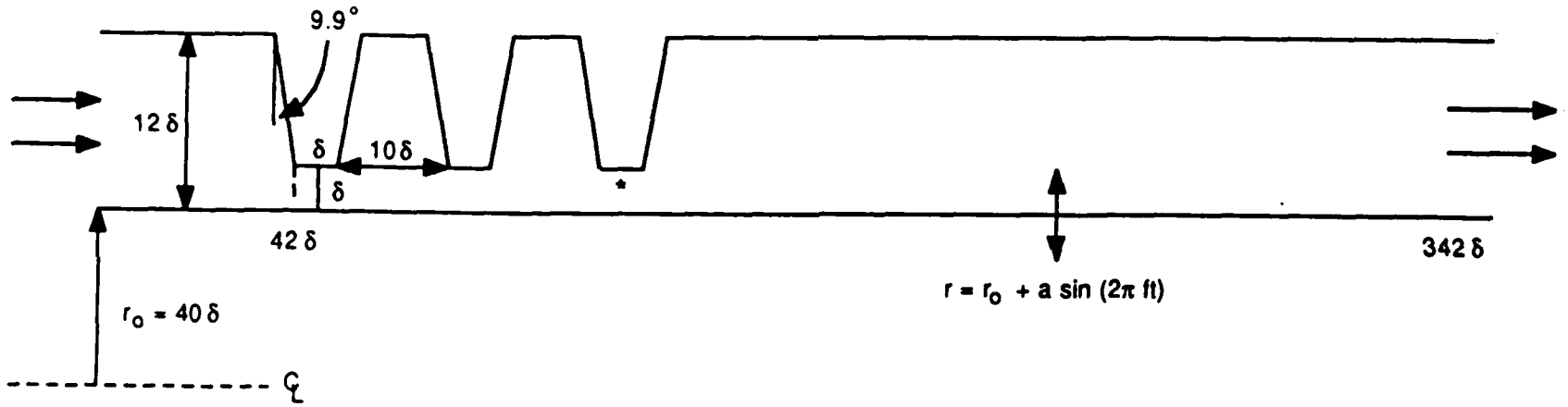

Figure 1. Straight tapered seal configuration.

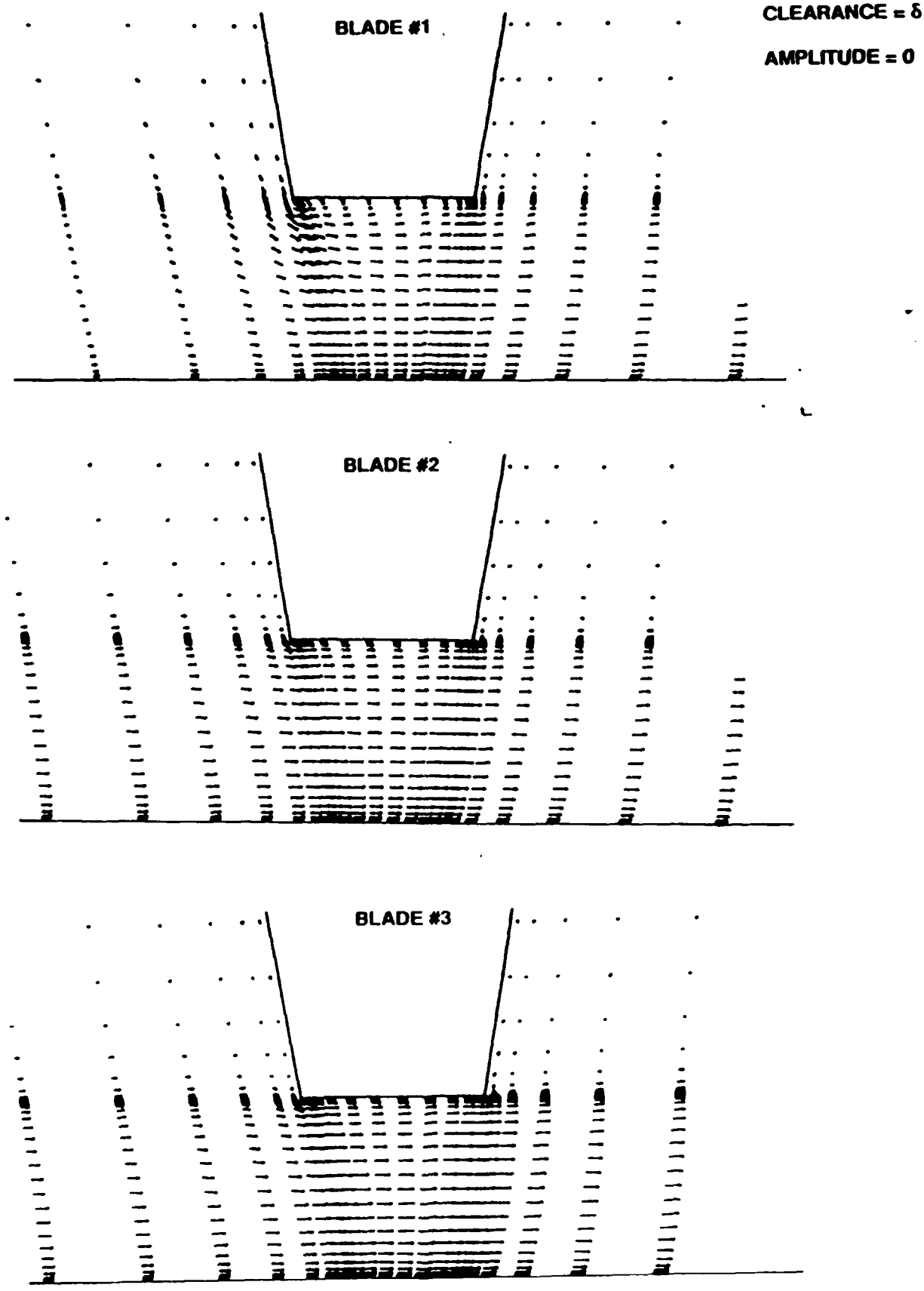

Figure 2. Case 1 - Velocity vectors inside the blade gap.

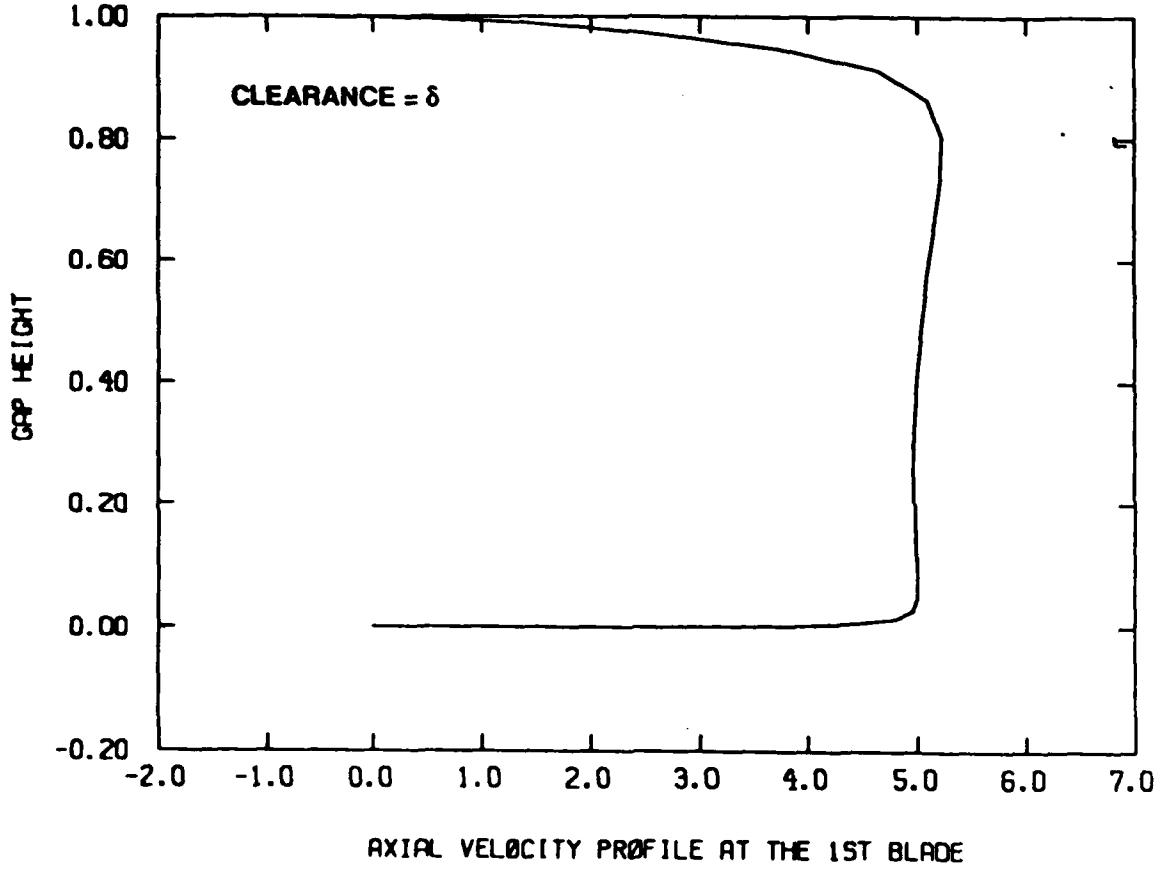

Figure 3. Case 1 - Velocity profile at the first blade gap.

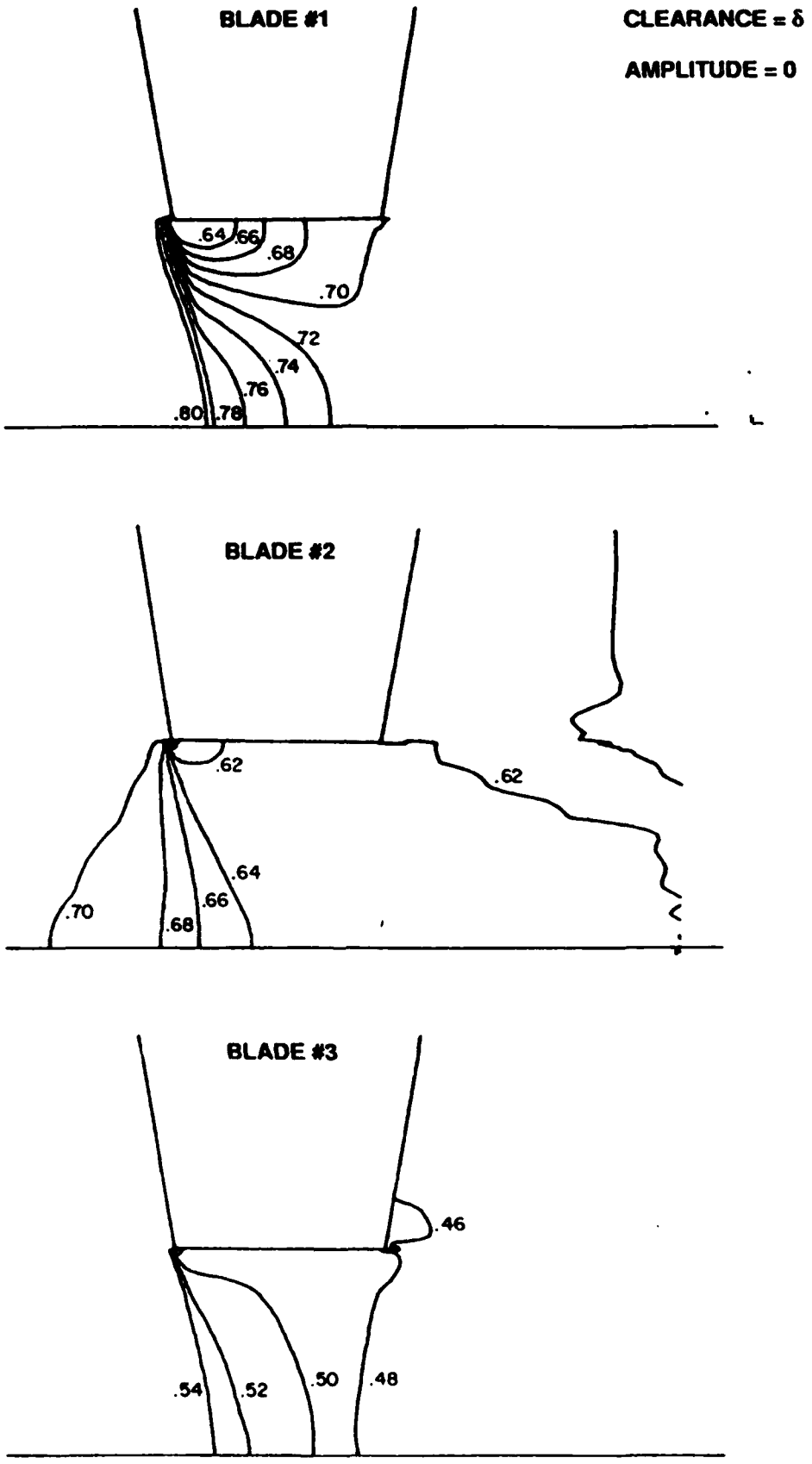

Figure 4. Case 1 - Pressure contours inside the blade gaps.

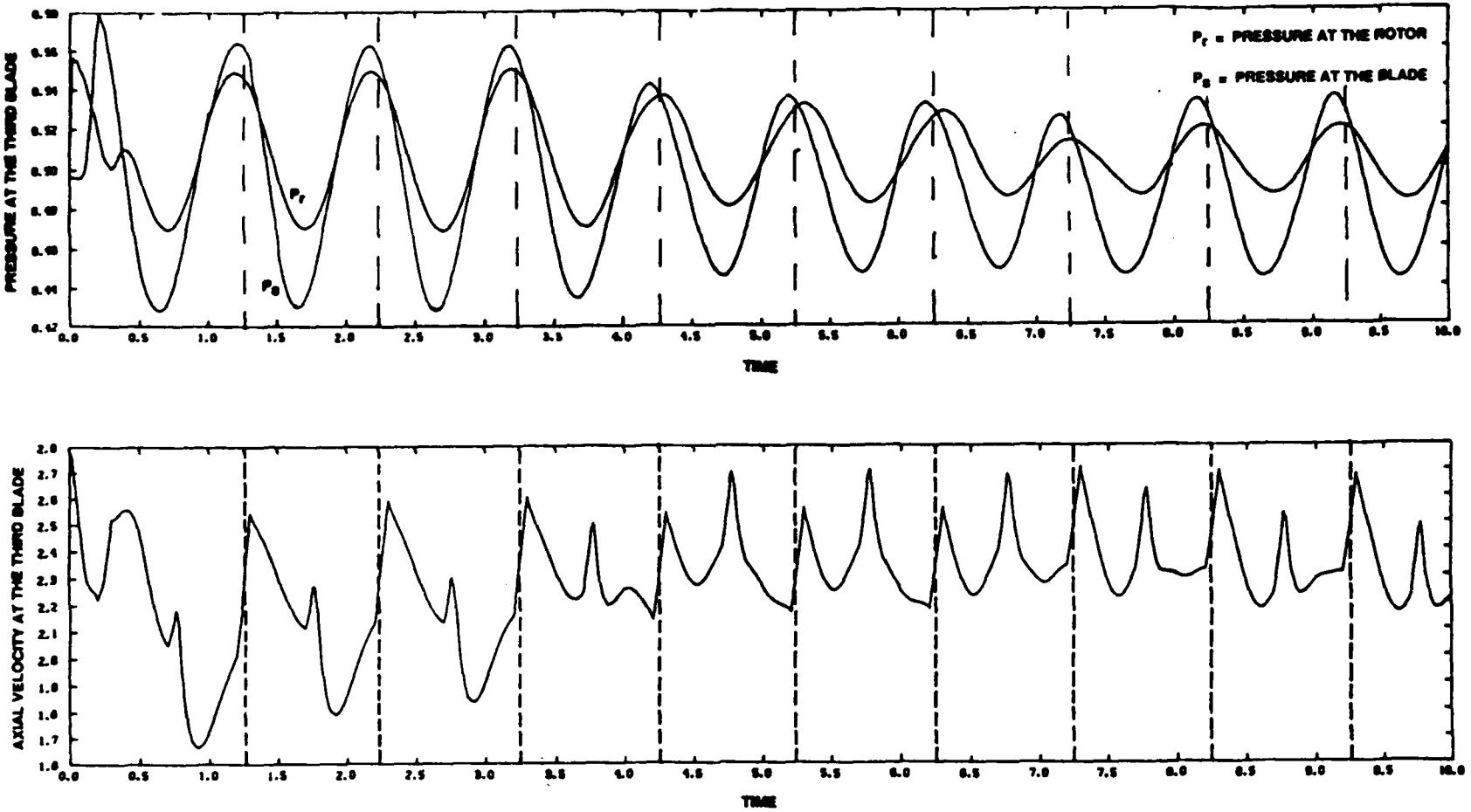

Figure 5. Case 2 - Pressure and axial velocity near the middle of the third blade vs. time.

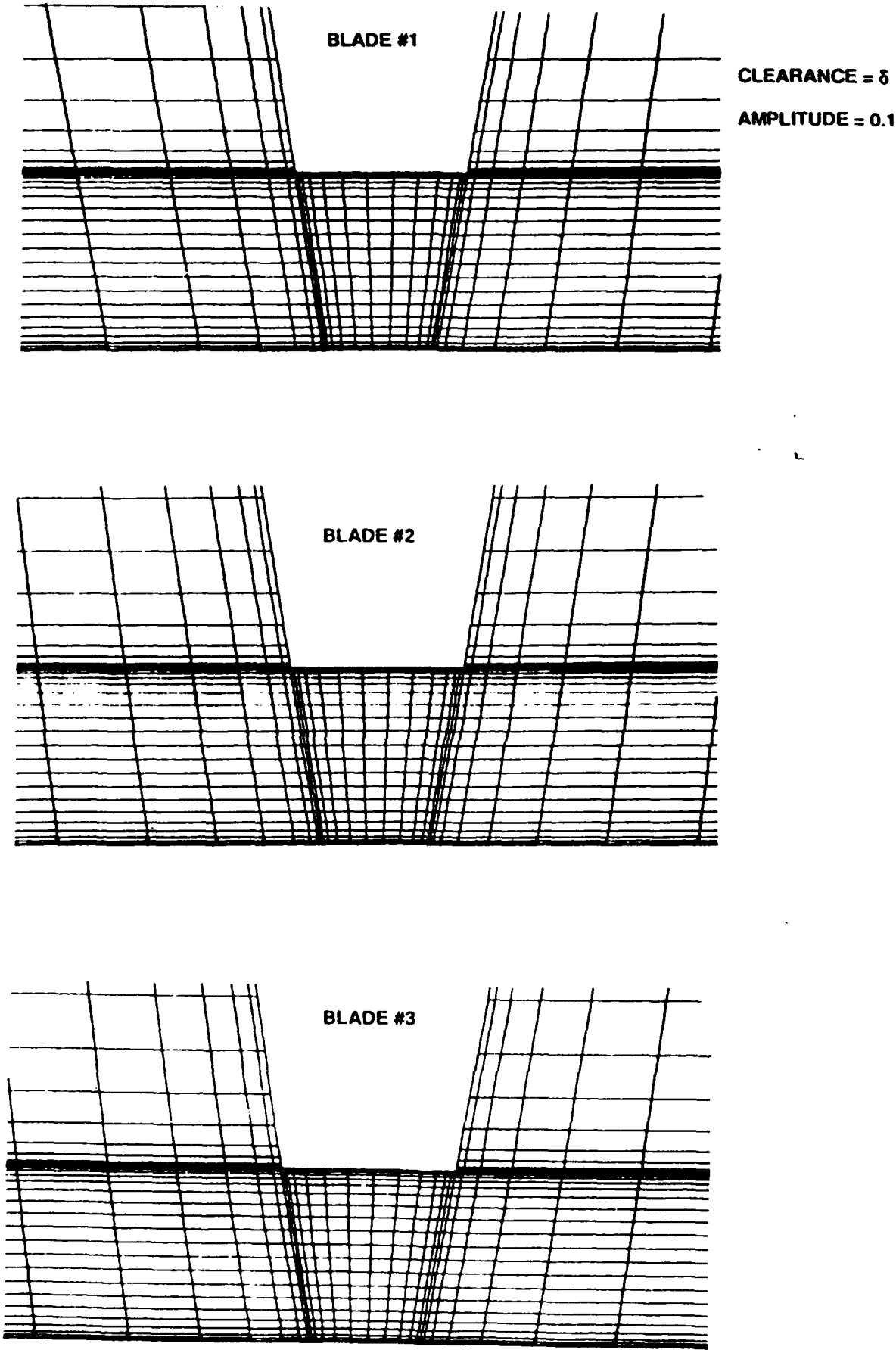

Figure 6. Case 2 - Coordinates inside the blade gaps at t = 9.00.

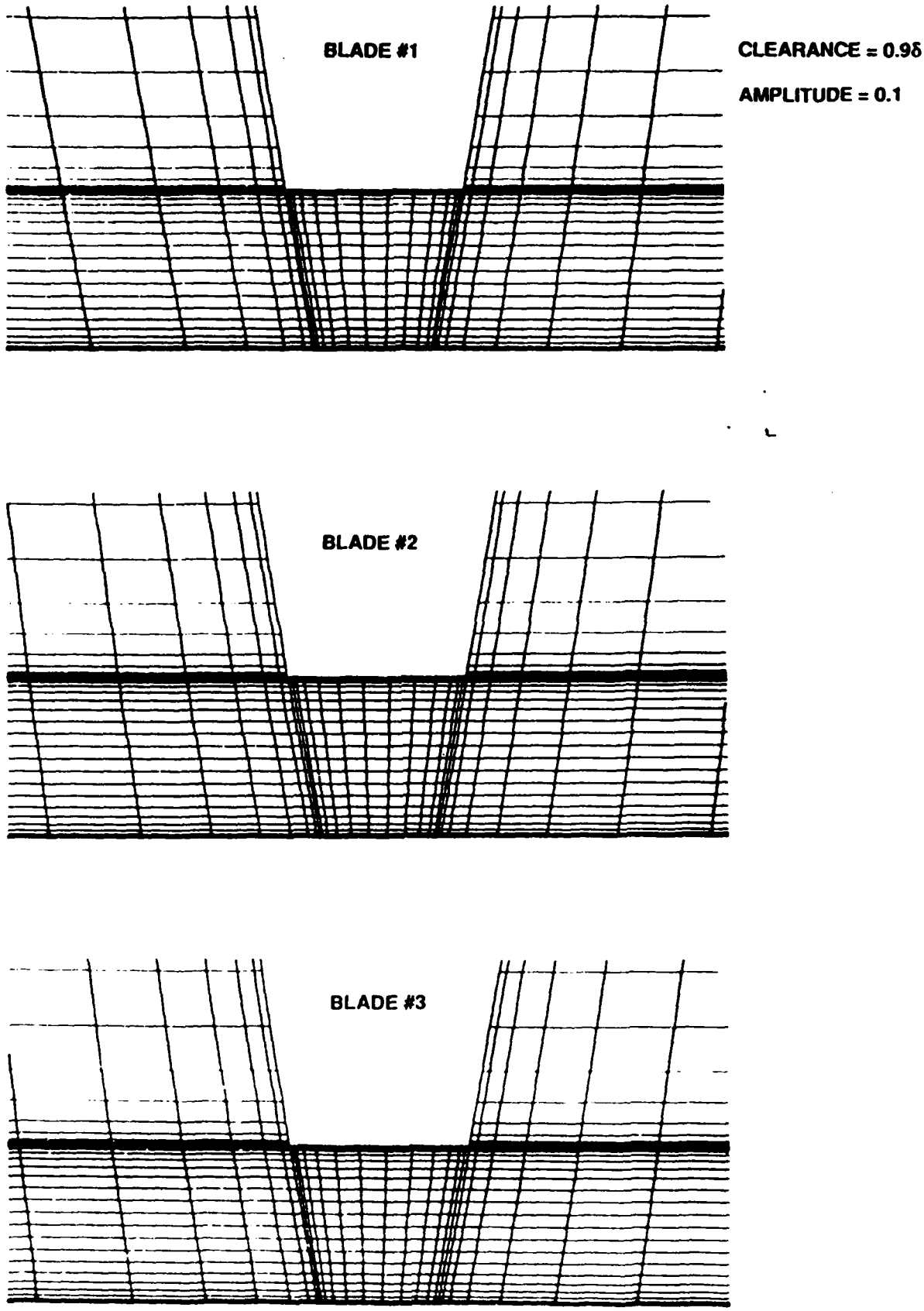

Figure 7. Case 2 - Coordinates inside the blade gaps at t = 9.25.

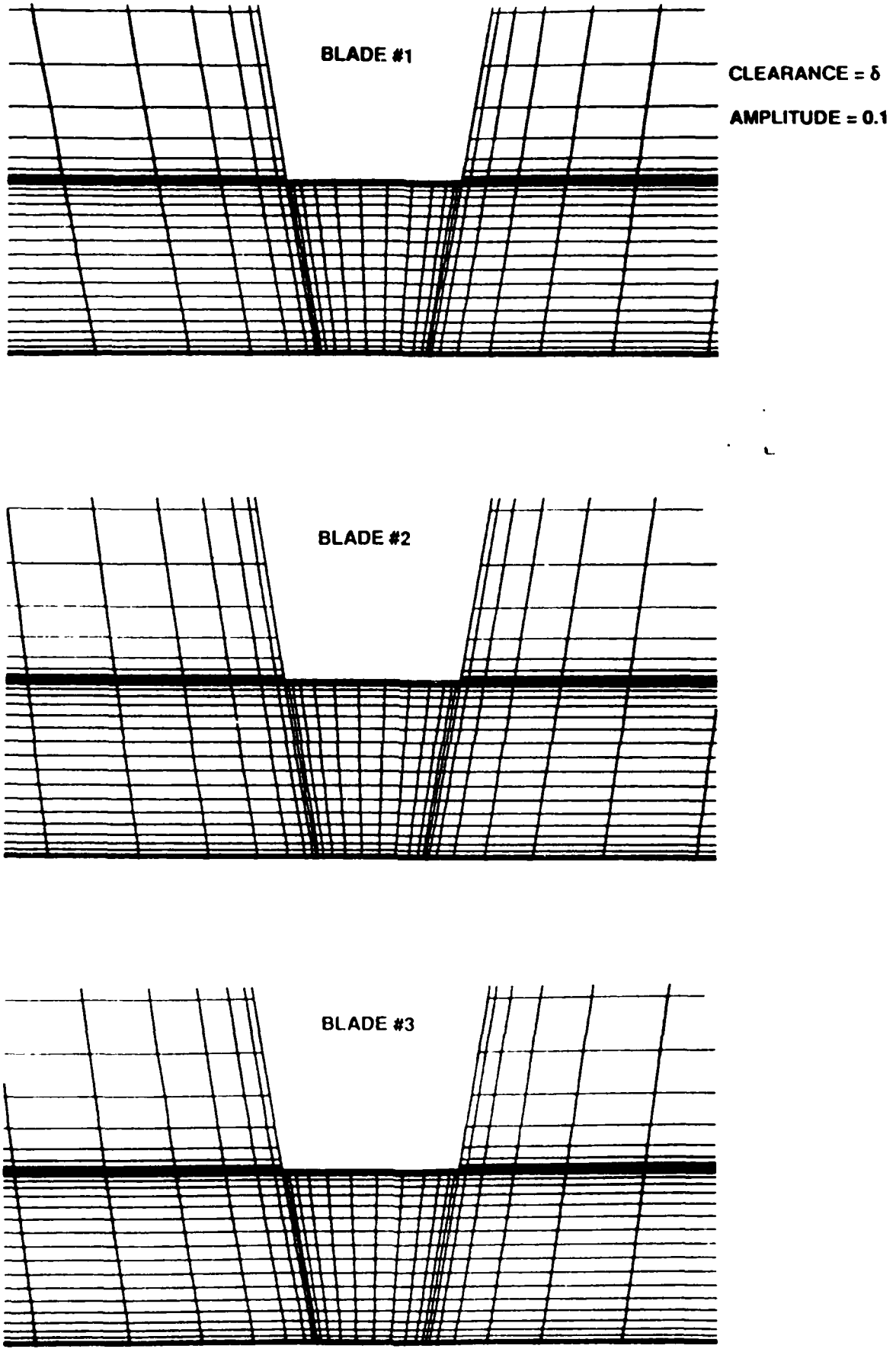

Figure 8. Case 2 - Coordinates inside the blade gaps at t = 9.50.

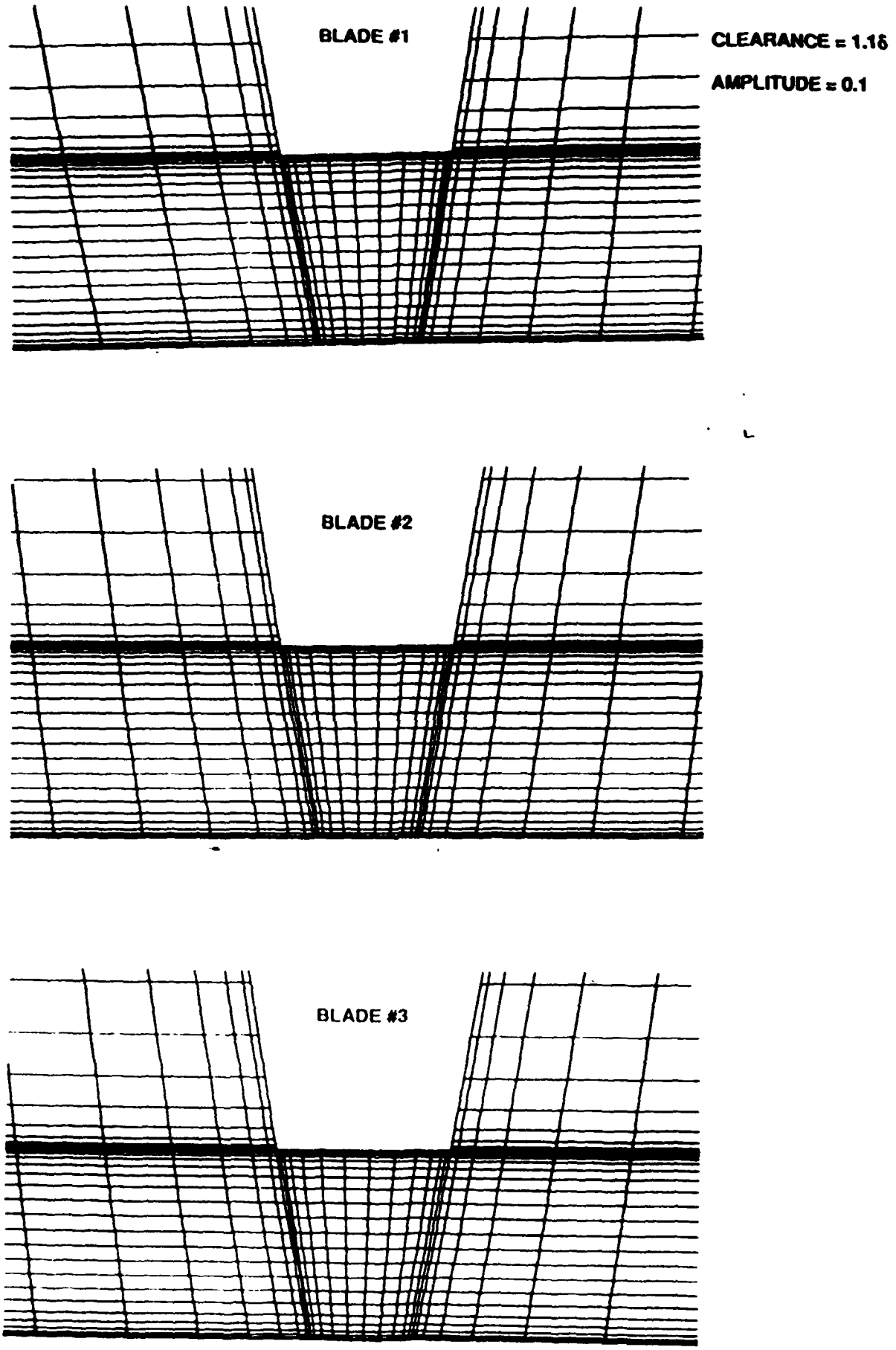

Figure 9. Case 2 - Coordinates inside the blade gaps at t = 9.75.

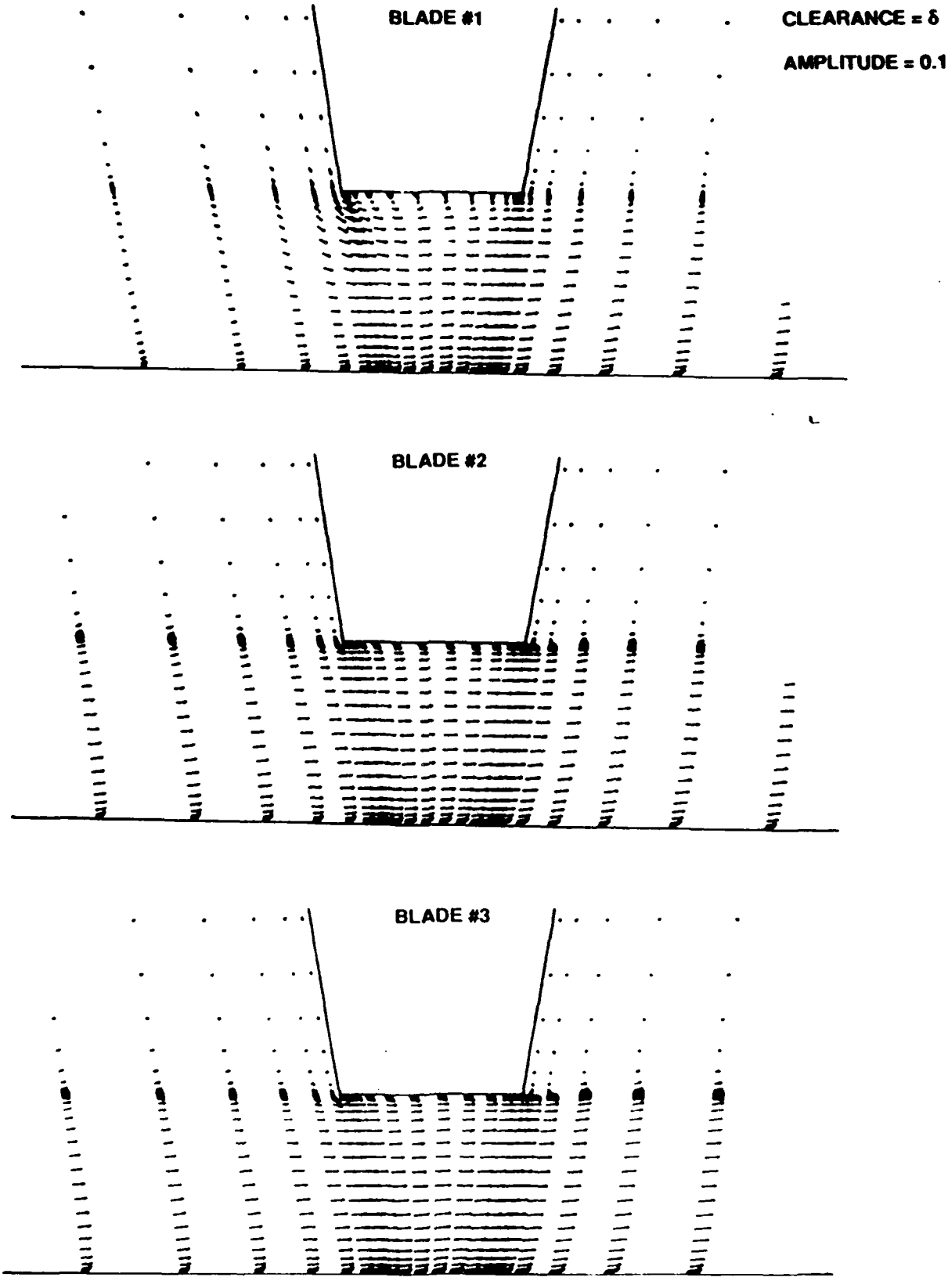

Figure 10. Case 2 - Velocity vectors inside the blade gaps at t = 9.00.

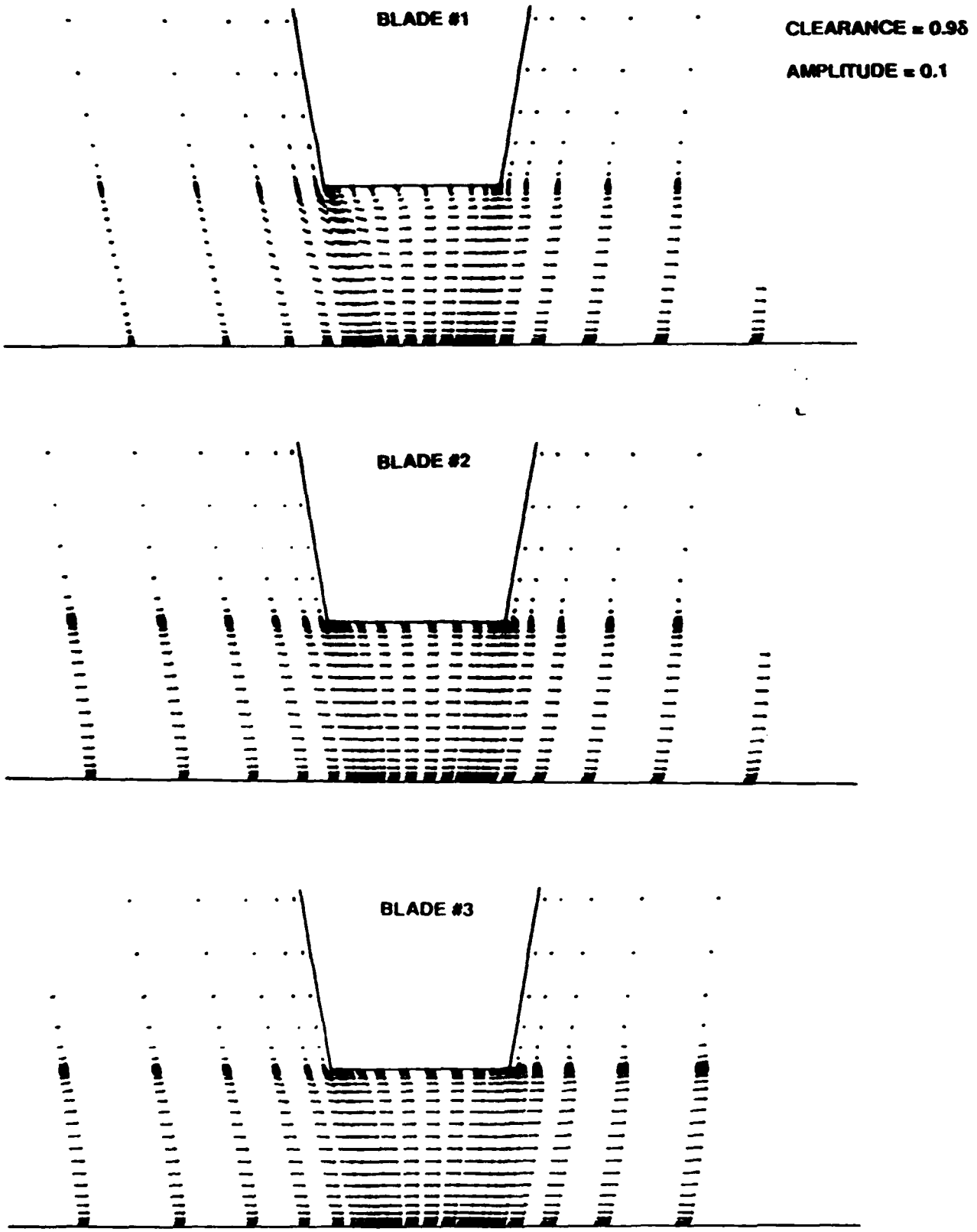

Figure 11. Case 2 - Velocity vectors inside the blade gaps at t = 9.25.

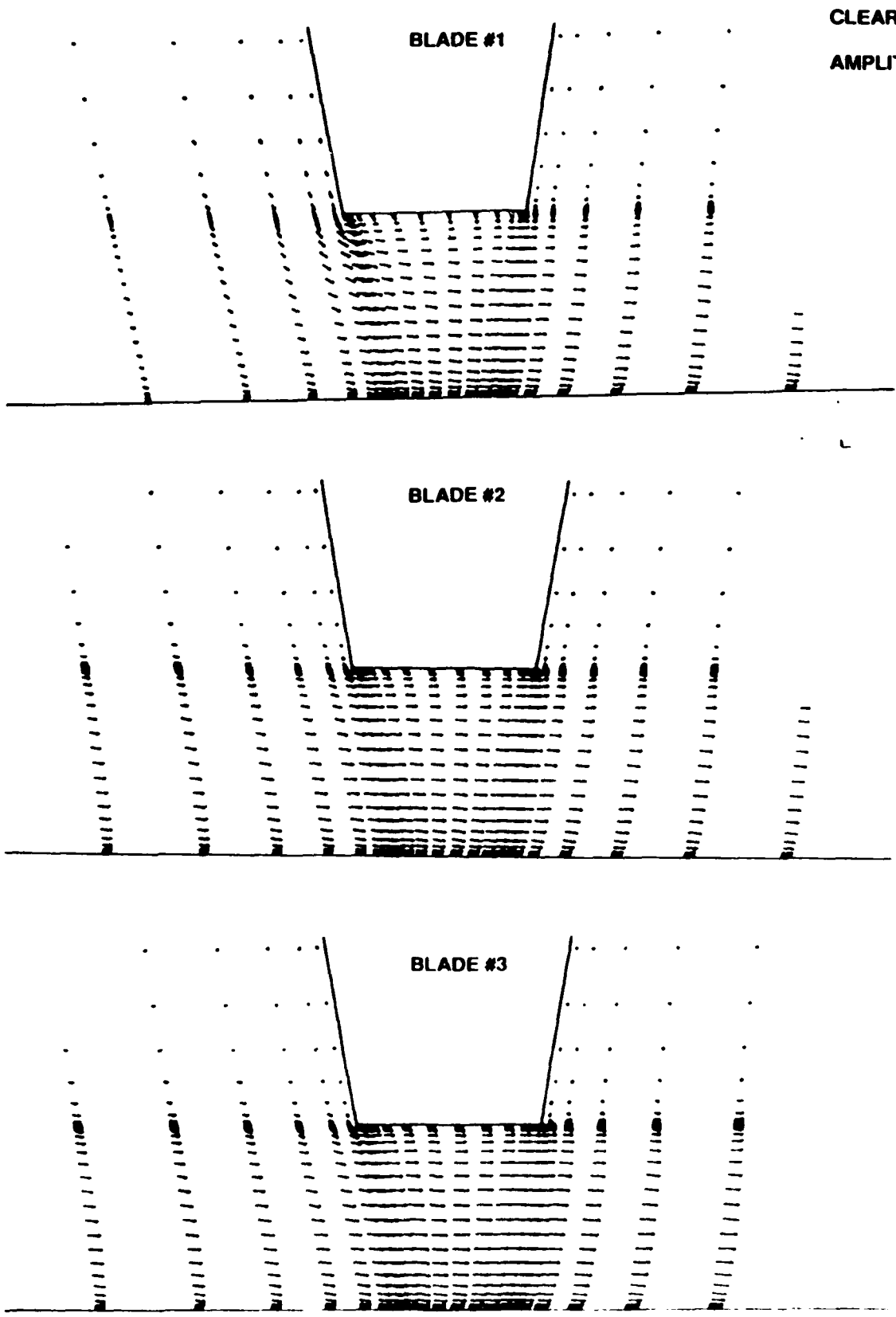

Figure 12. Case 2 - Velocity vectors inside the blade gaps at t = 9.50.

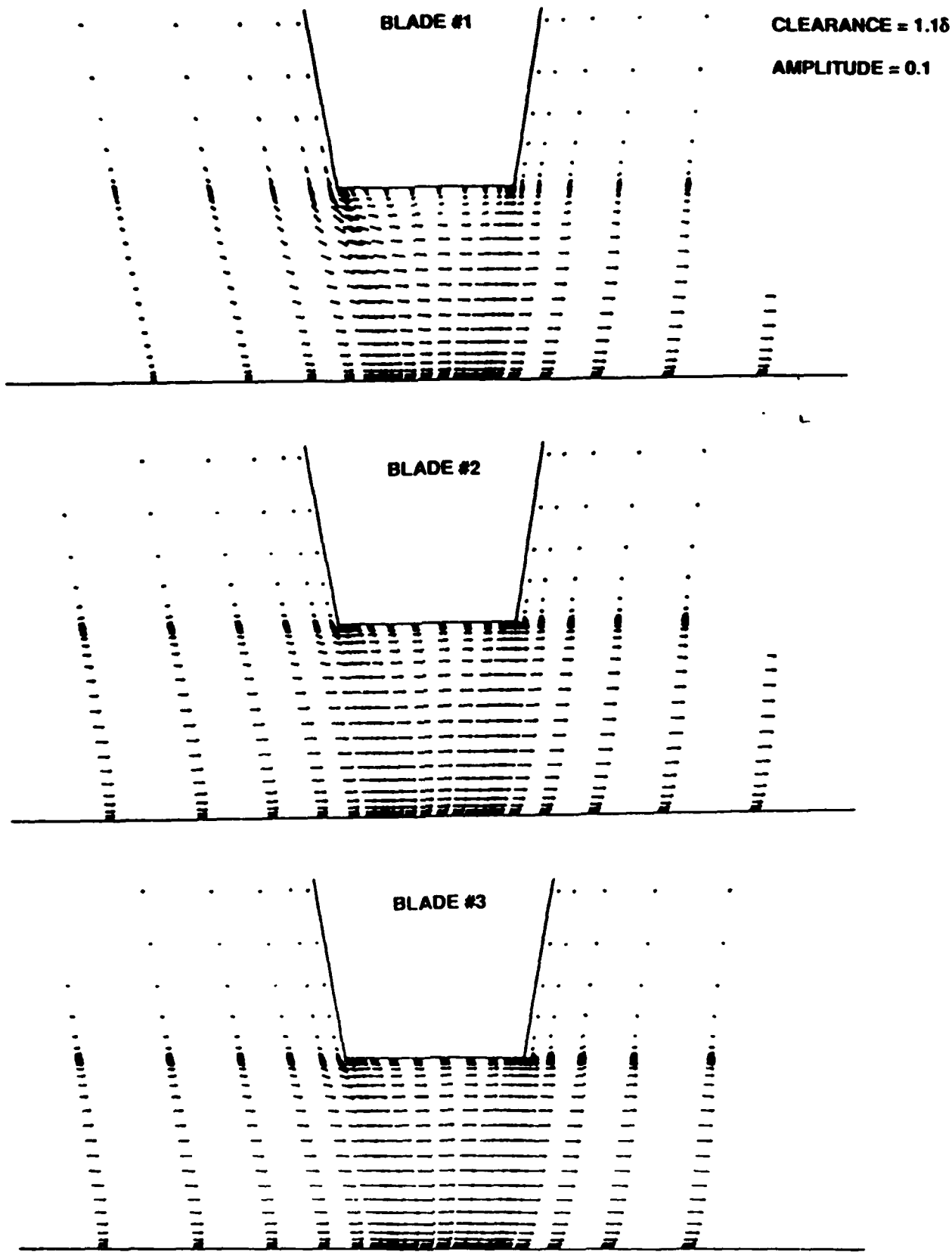

Figure 13. Case 2 - Velocity vectors inside the blade gaps at t = 9.75.

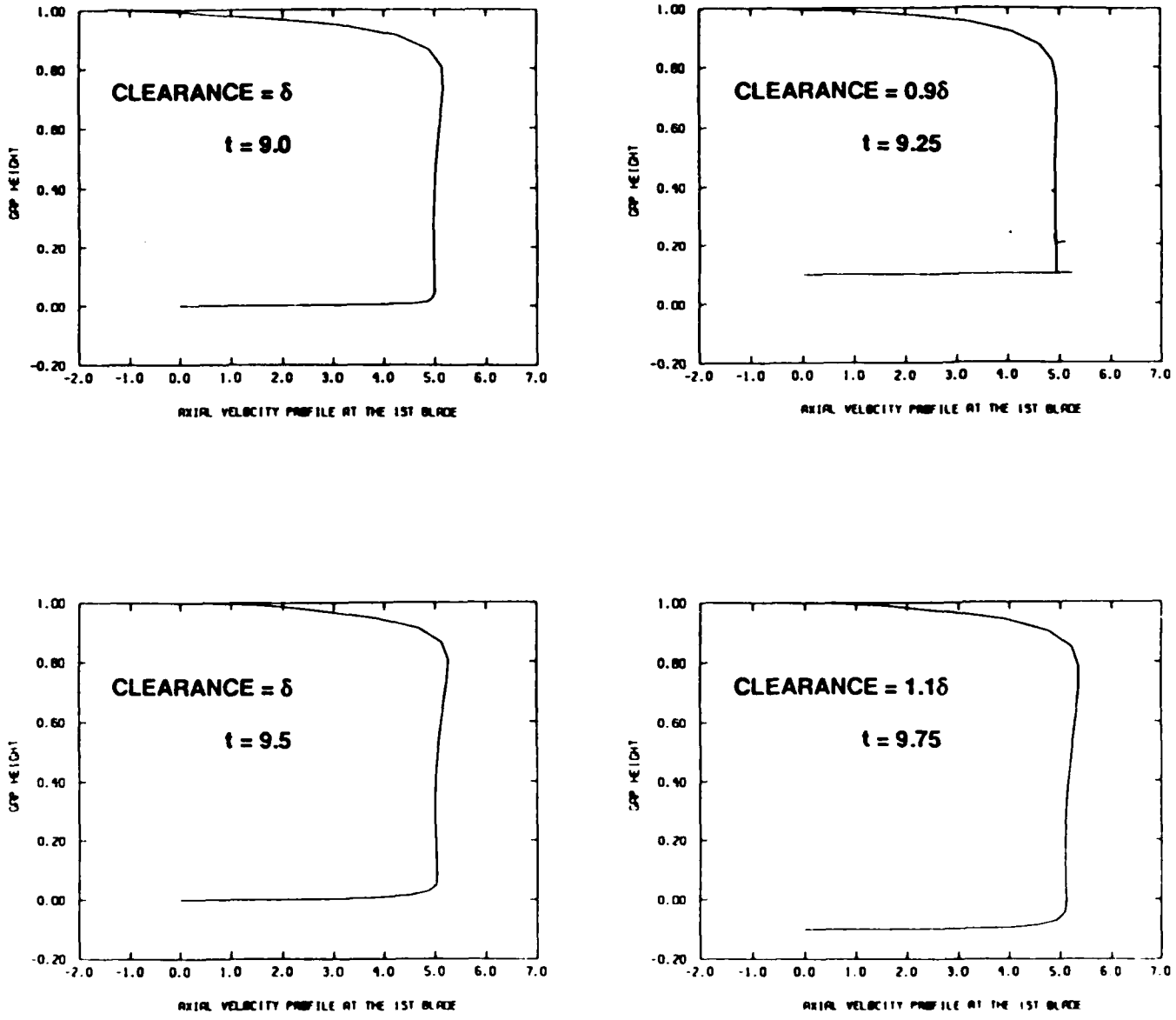

Figure 14. Case 2 - Velocity profiles inside the first blade gap.

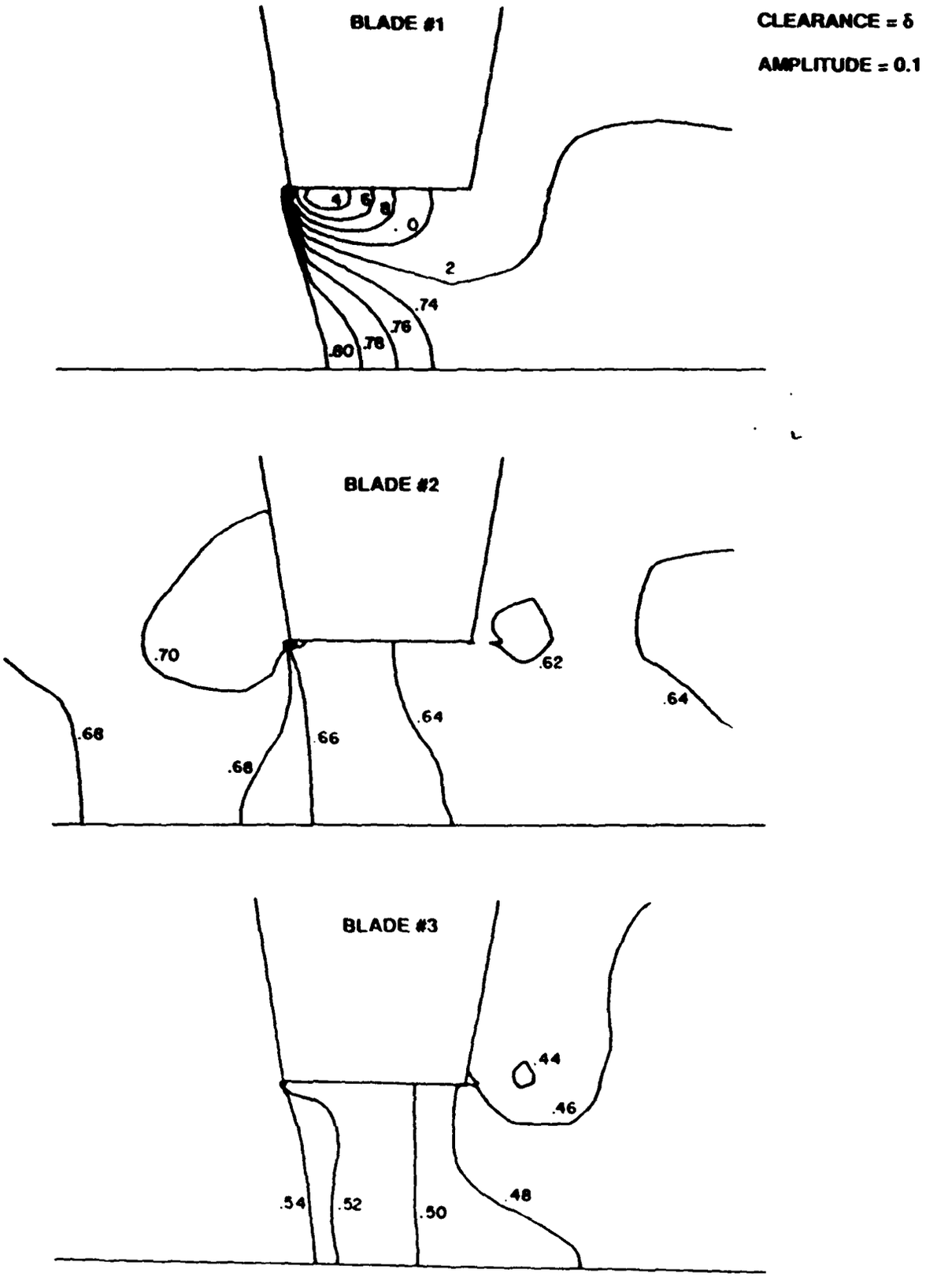

Figure 15. Case 2 - Pressure contours inside the blade gaps at t = 9.00.

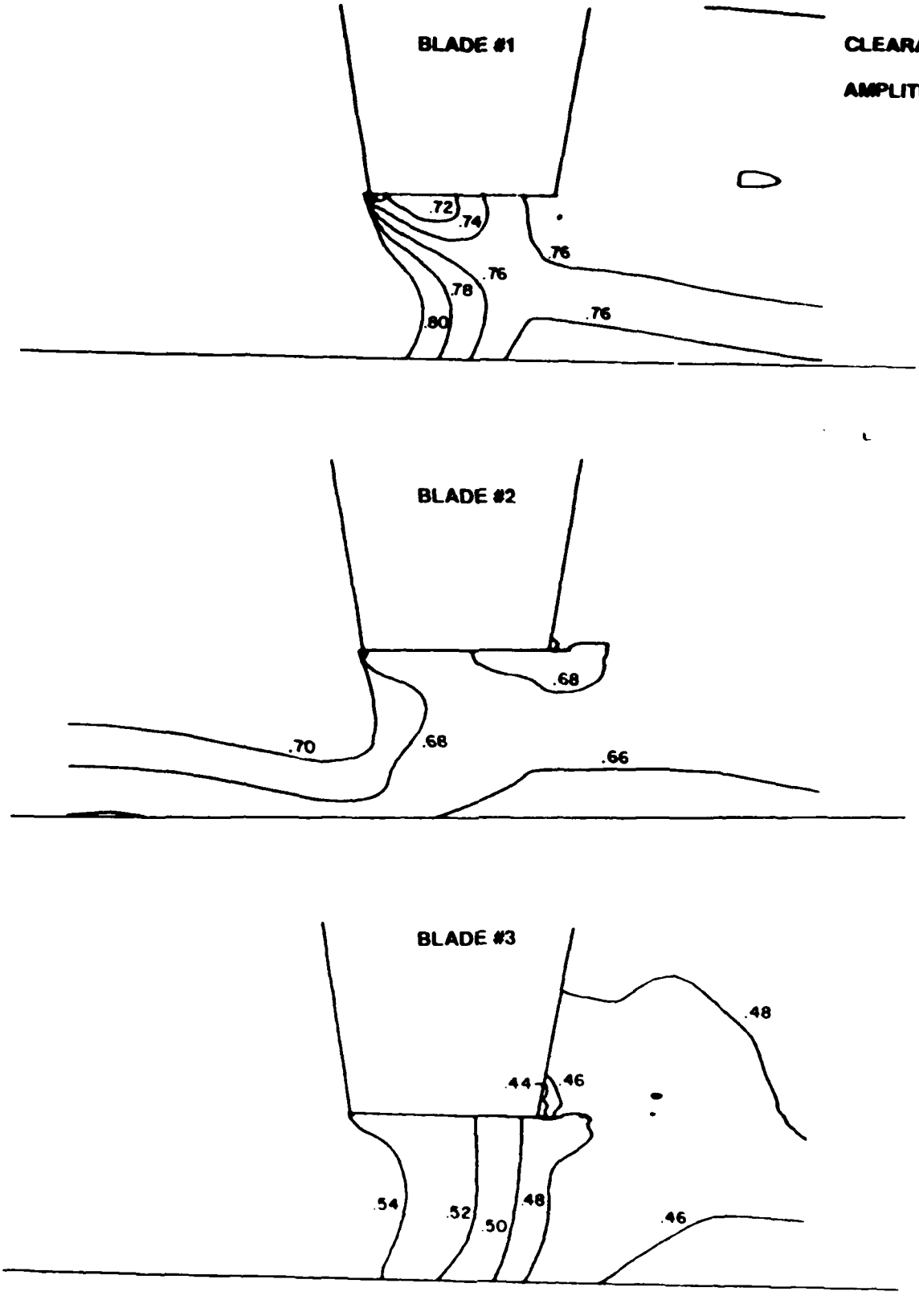

Figure 16. Case 2 - Pressure contours inside the blade gaps at t = 9.25.

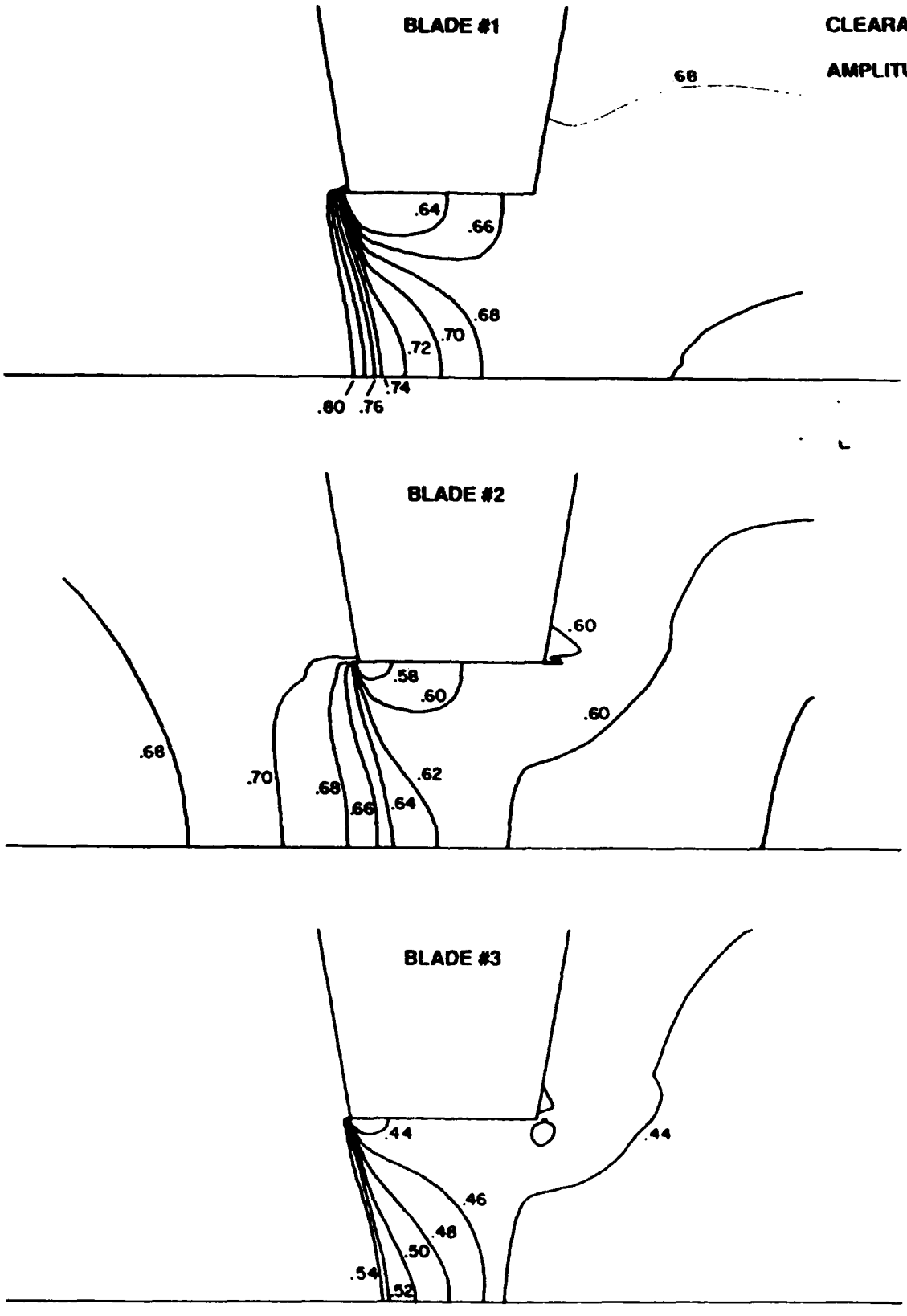

Figure 17. Case 2 - Pressure contours inside the blade gaps at t = 9.50.

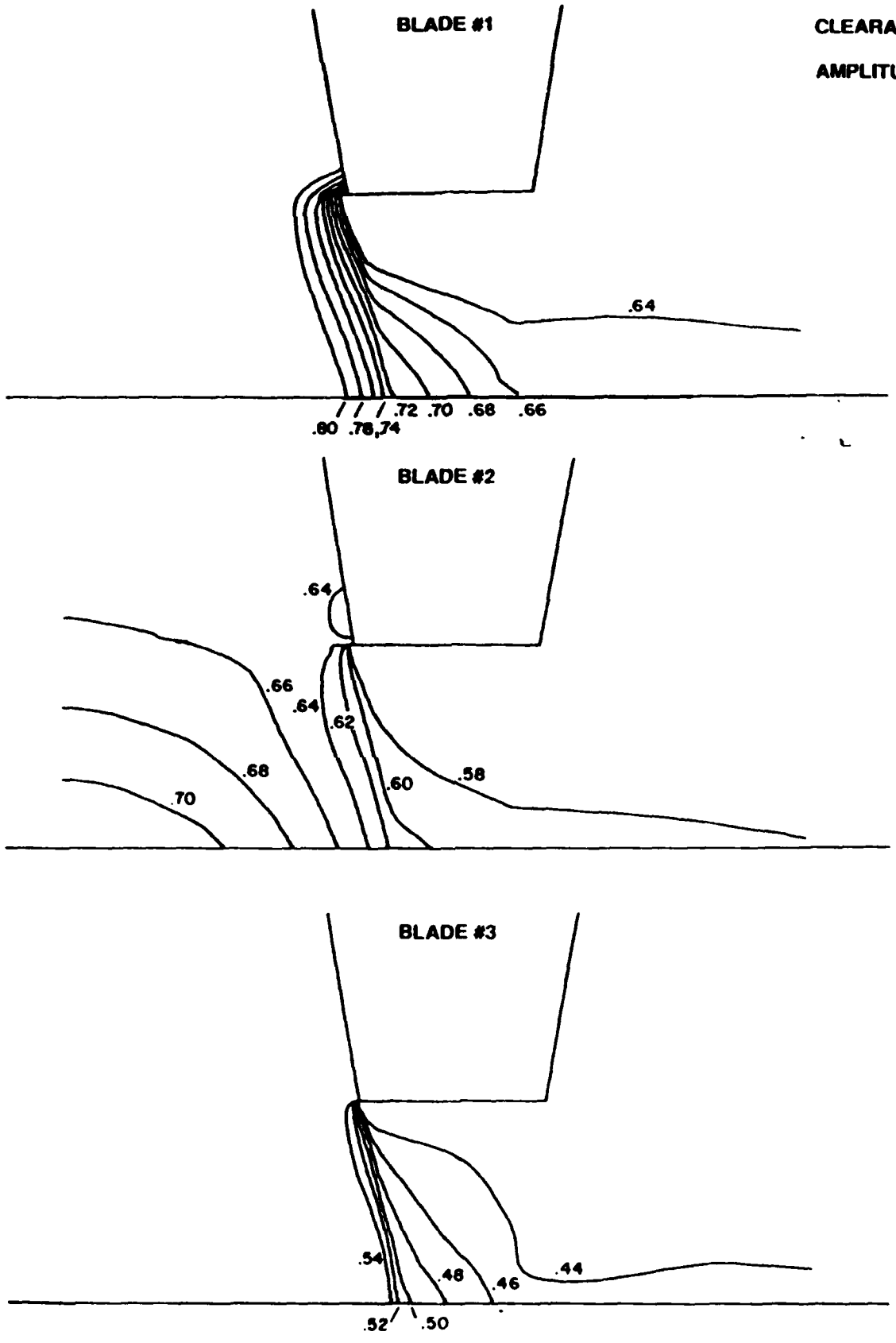

Figure 18. Case 2 - Pressure contours inside the blade gaps at t = 9.75.

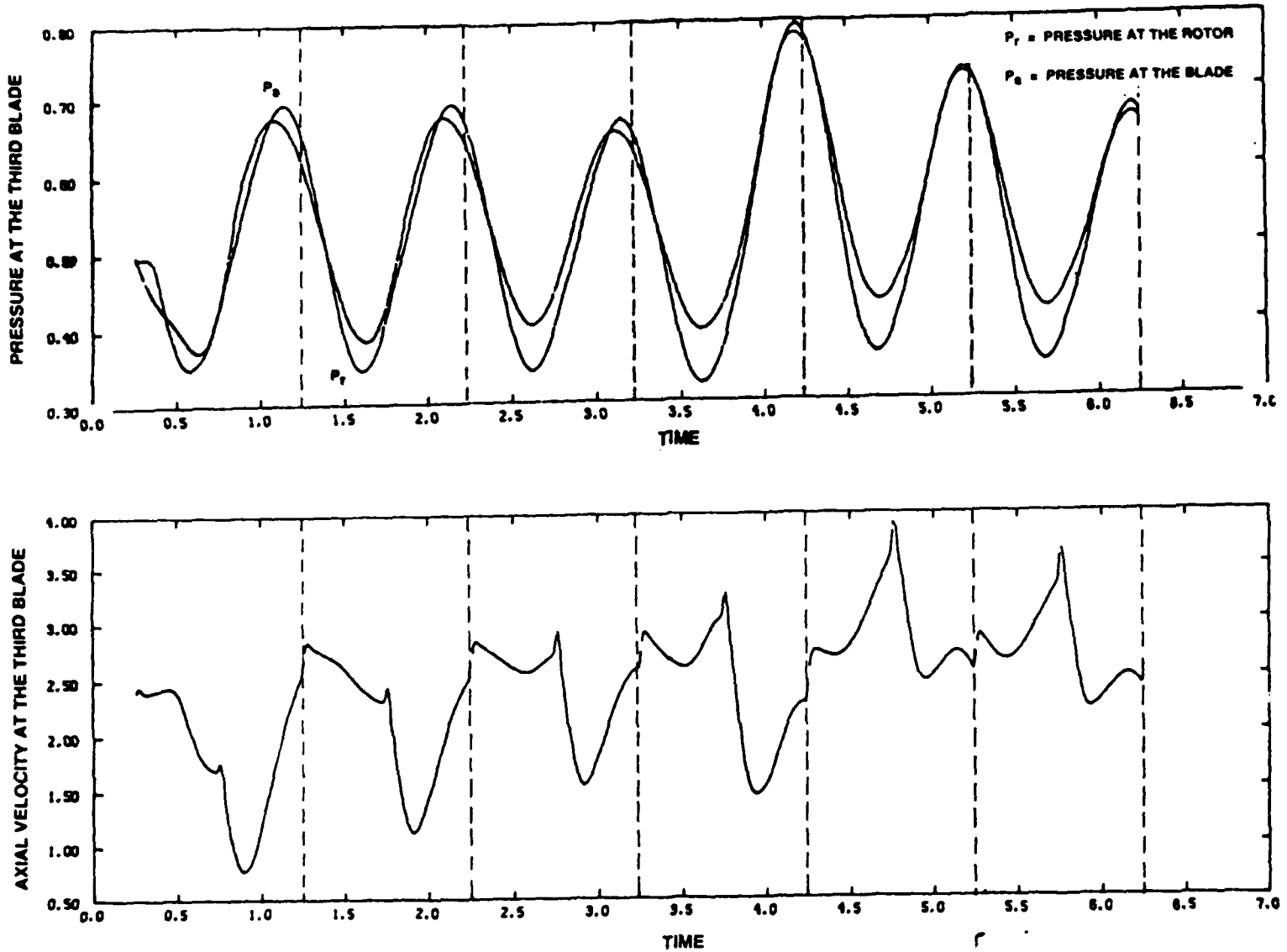

Figure 19. Case 3 - Pressure and axial velocity near the middle of the third blade vs. time.

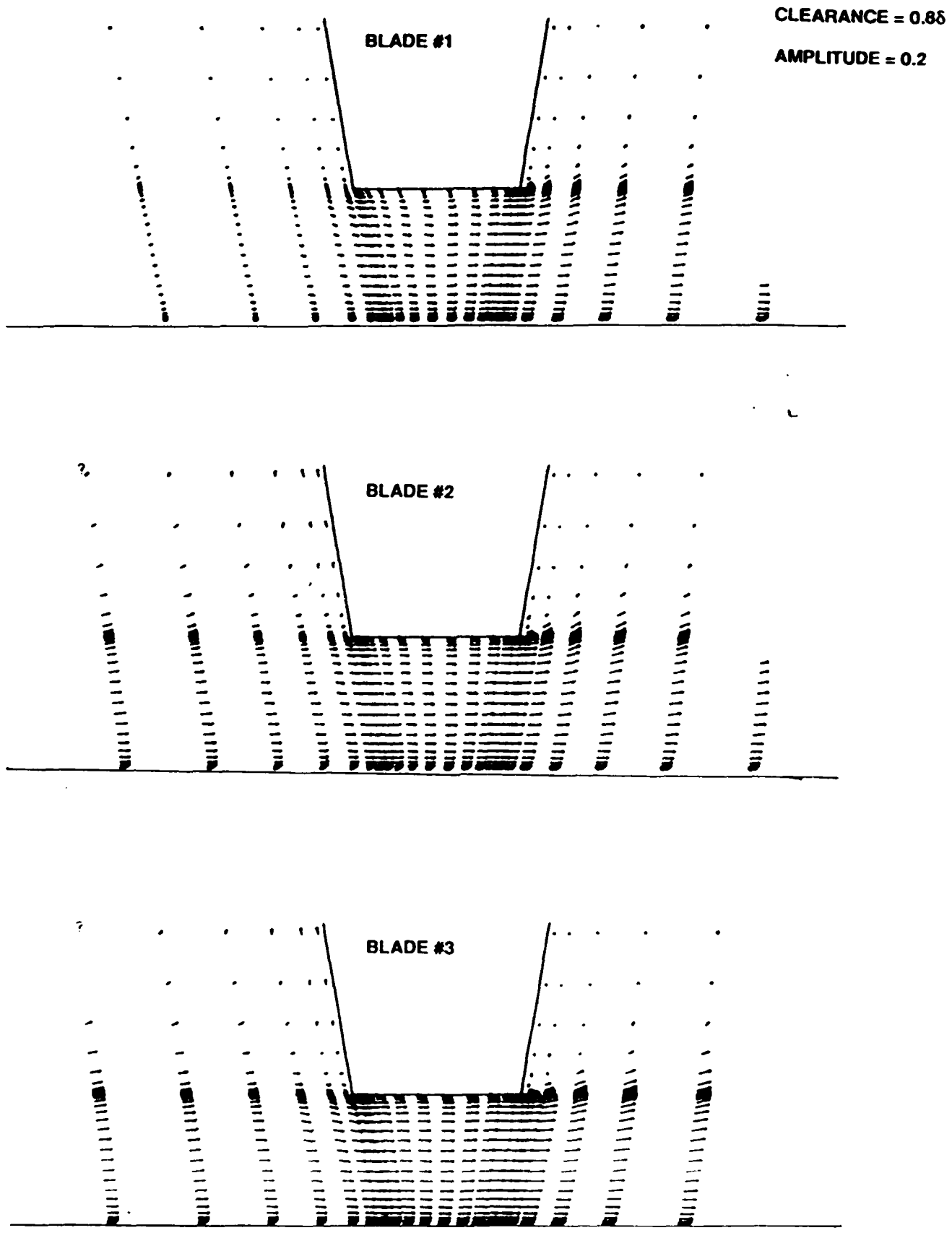

Figure 20. Case 3 - Velocity vectors inside the blade gaps at t = 4.25.

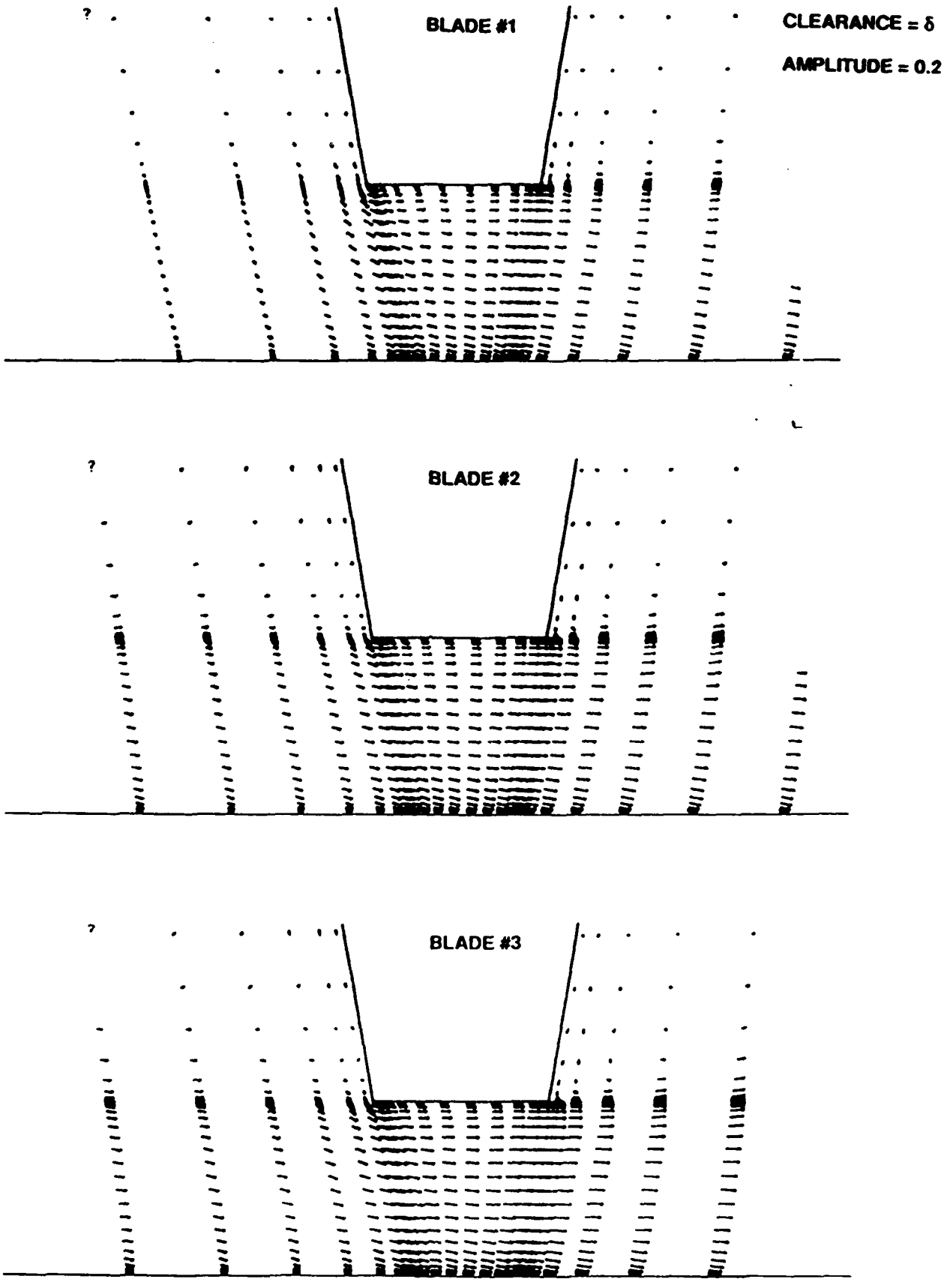

Figure 21. Case 3 - Velocity vectors inside the blade gaps at t = 4.50.

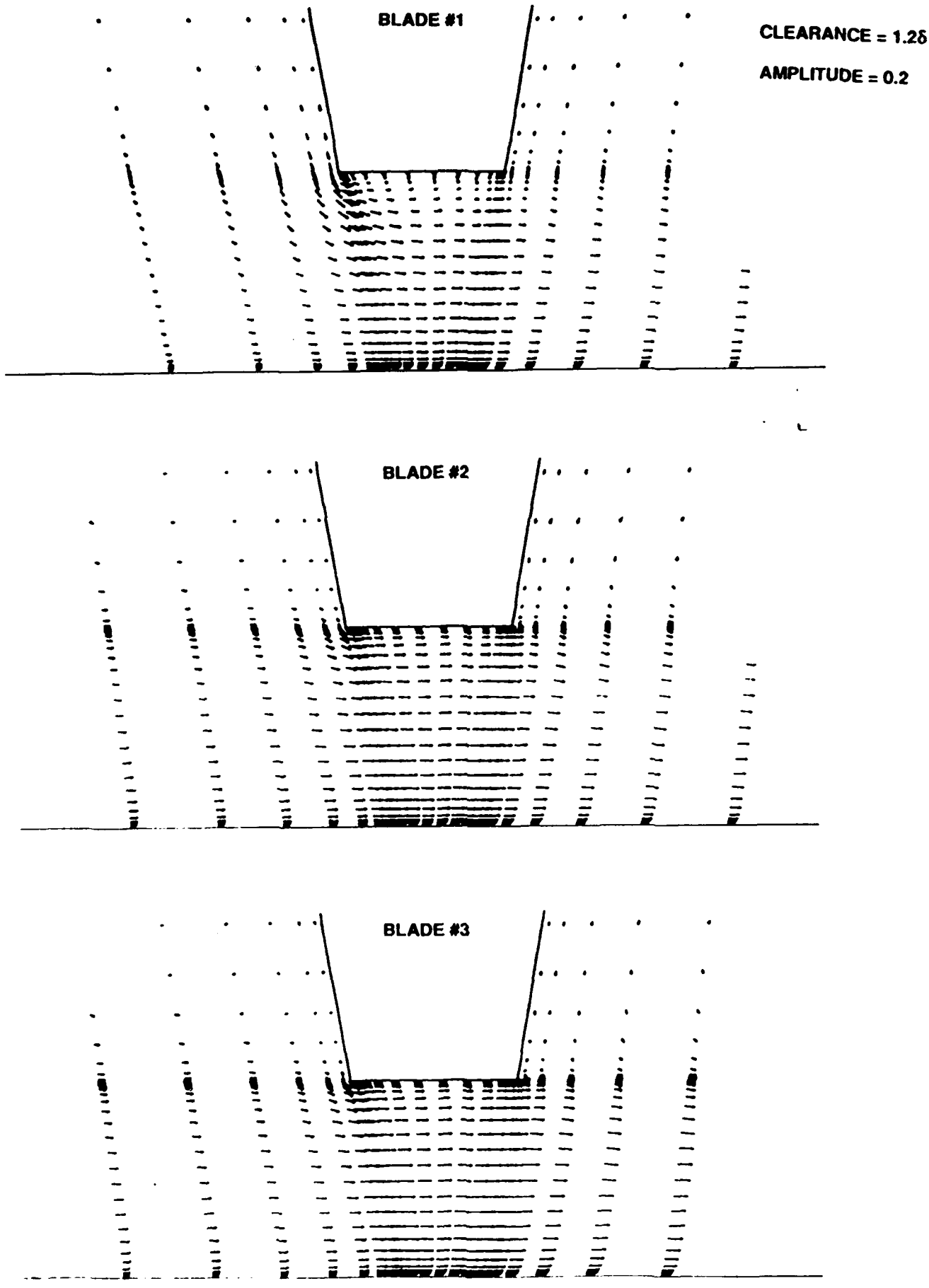

Figure 22. Case 3 - Velocity vectors inside the blade gaps at t = 4.75.

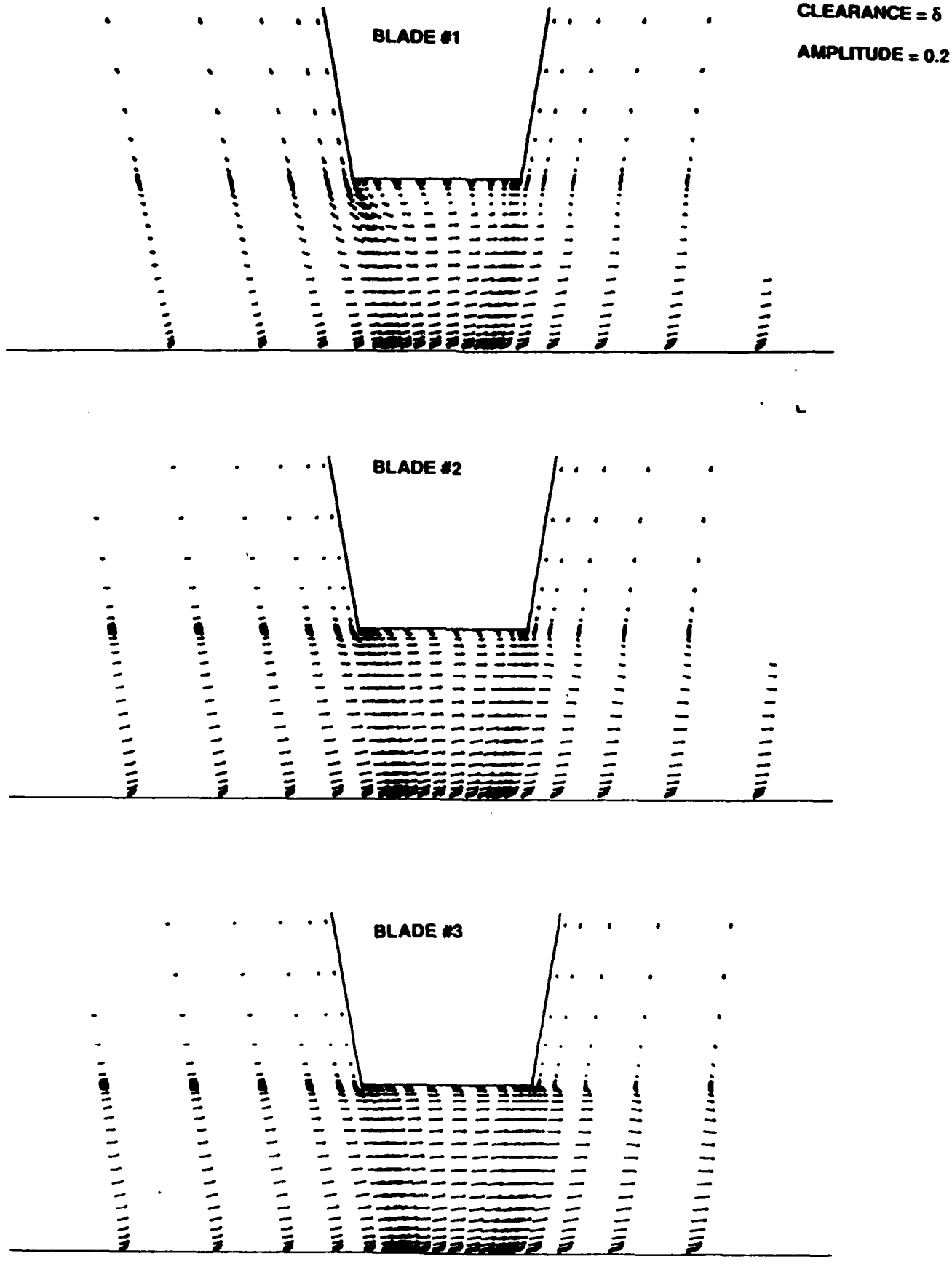

Figure 23. Case 3 - Velocity vectors inside the blade gaps at t = 5.00.

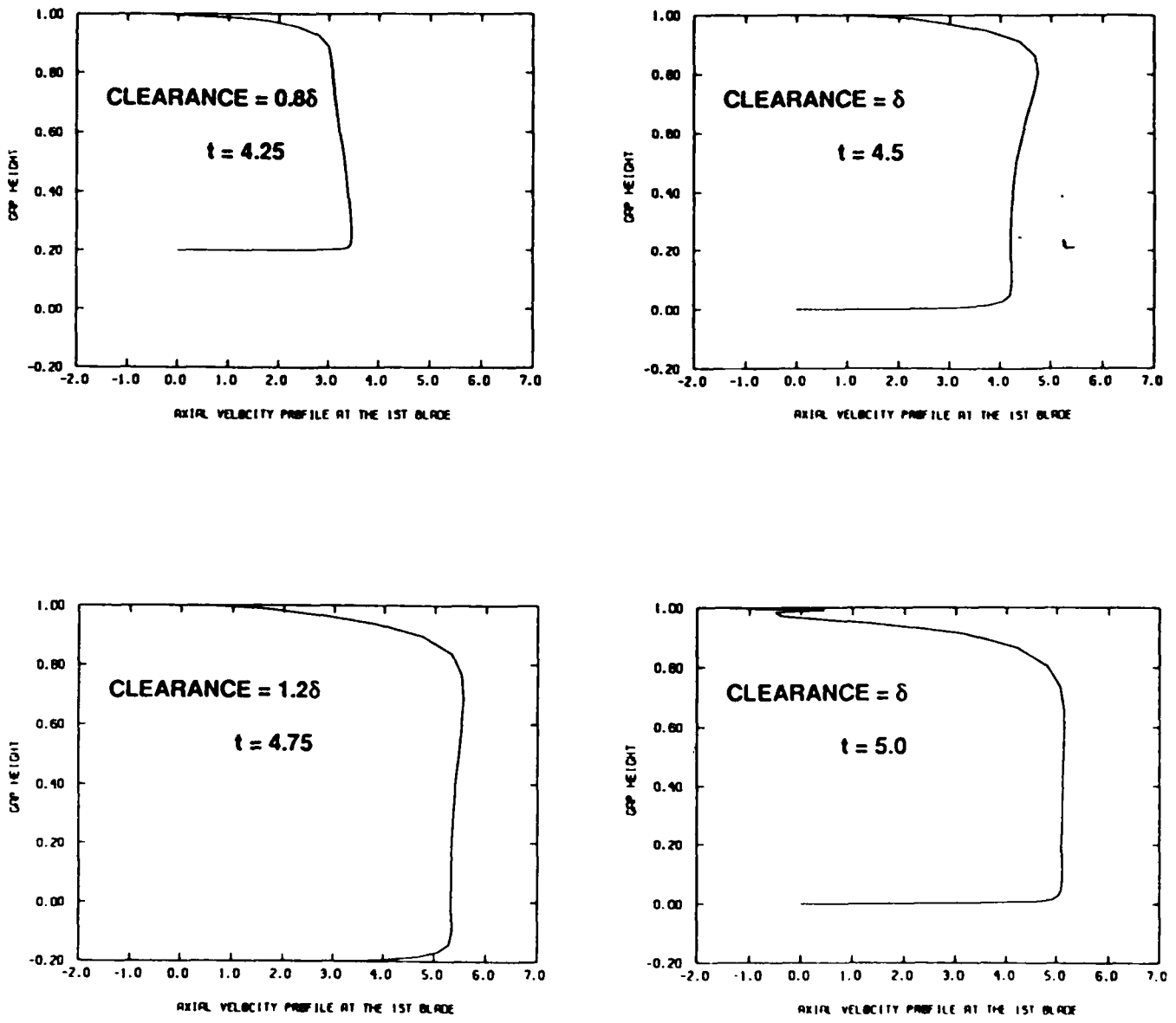

Figure 24. Case 3 - Velocity profiles inside the first blade gap.

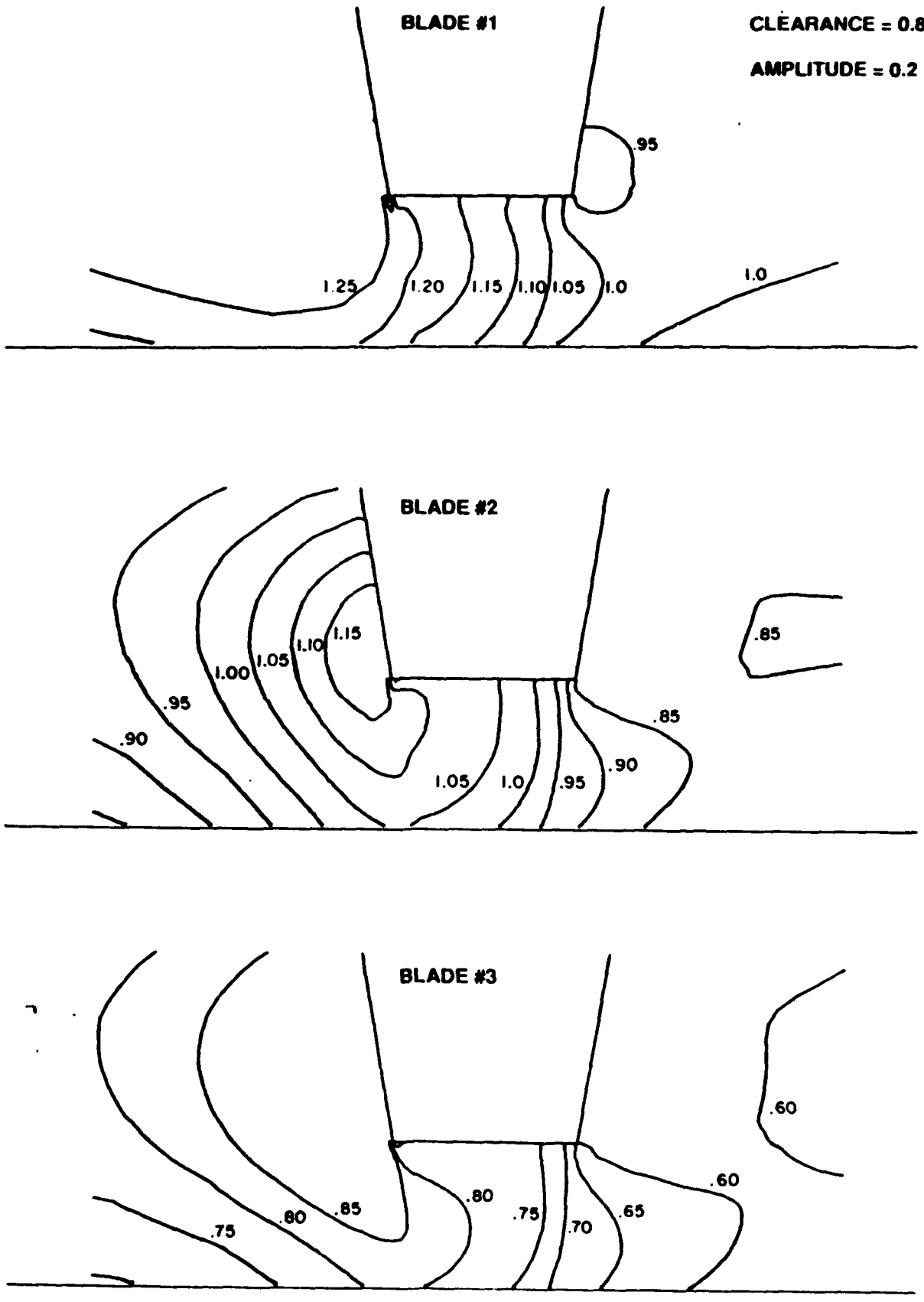

Figure 25. Case 3 - Pressure contours inside the blade gaps at t = 4.25.

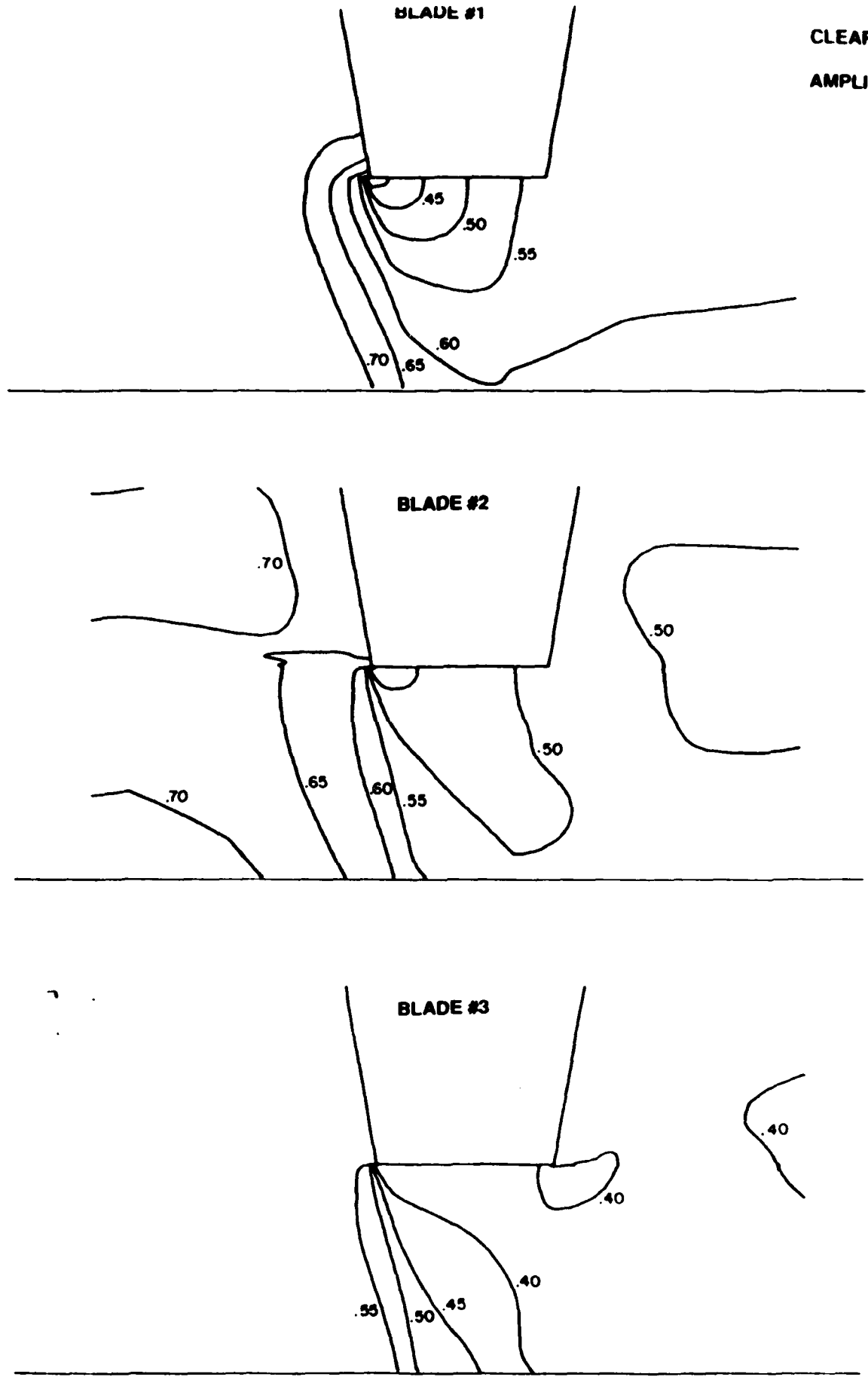

Figure 26. Case 3 - Pressure contours inside the blade gaps at t = 4.50.

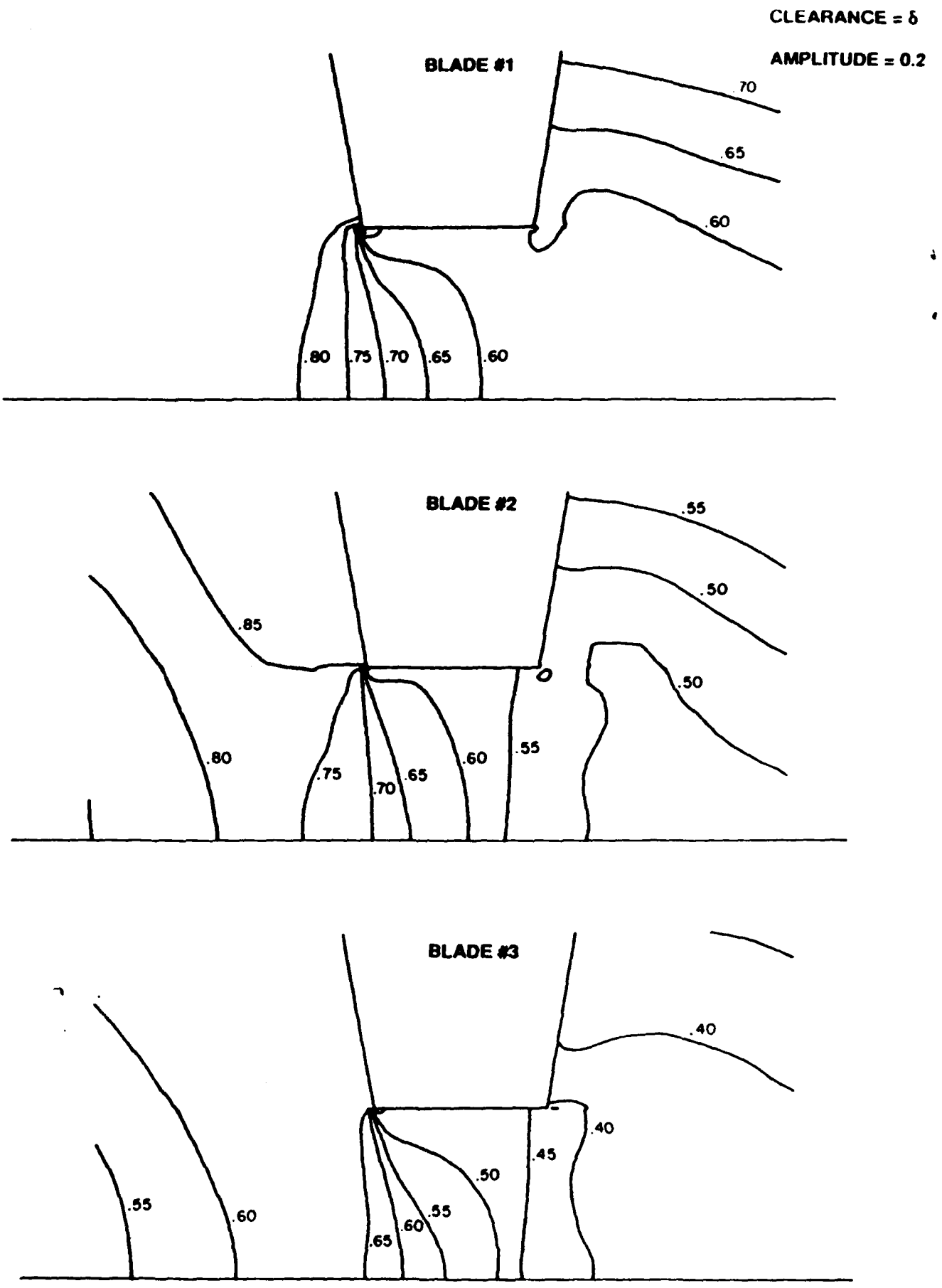

Figure 27. Case 3 - Pressure contours inside the blade gaps at t = 4.75.

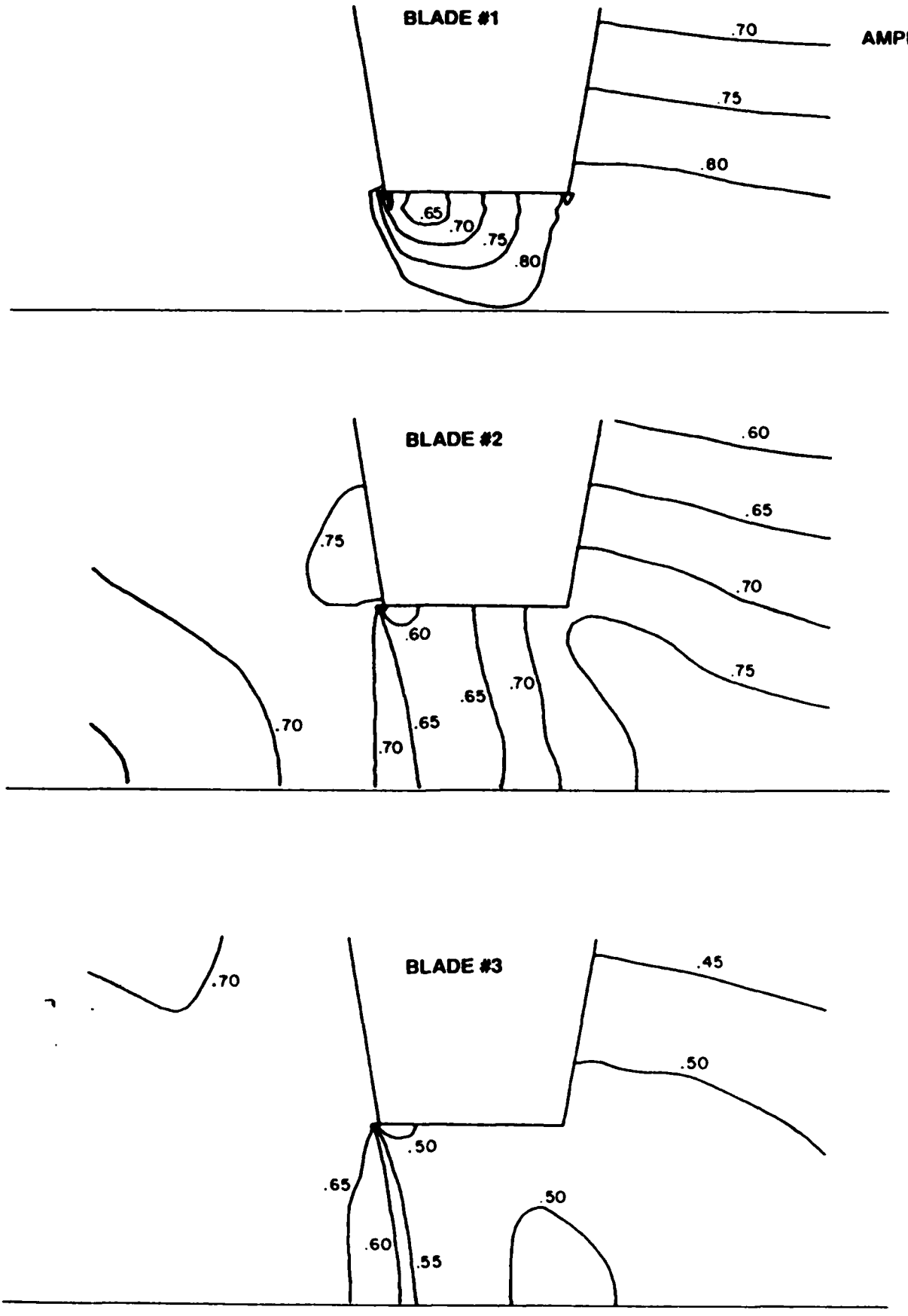

Figure 28. Case 3 - Pressure contours inside the blade gaps at t = 5.00.

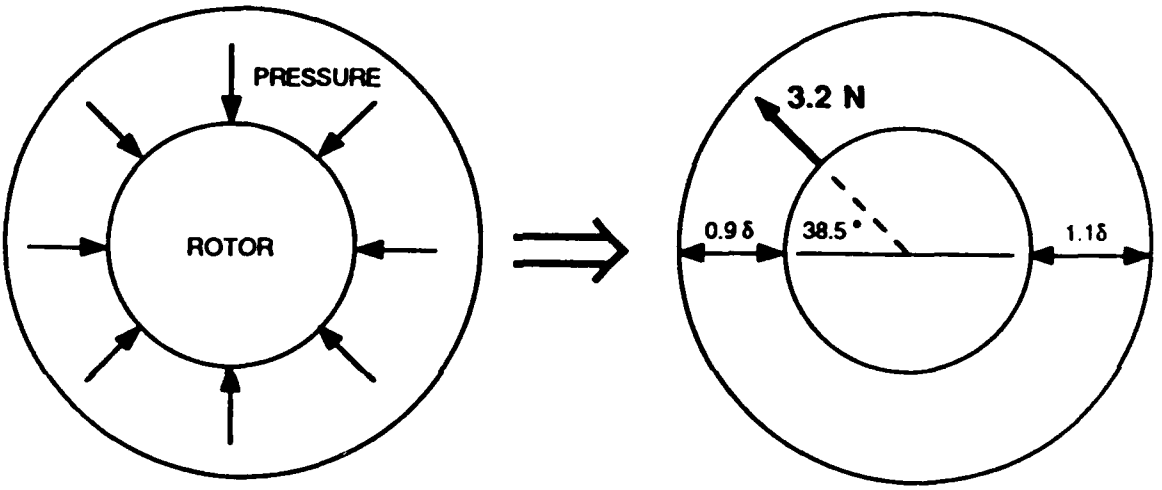

Figure 29. Net force acting on the rotor.

U.S.Government Printing Office: 1987 — 748-061/61089

END

11-87

DTIC